Global Biogeochemical Cycles

RESEARCH ARTICLE
10.1029/2025GB008531

High Lithogenic and Micro-Nutrient Fluxes From the West Greenland Margin Traced by Thorium in Seawater and Sediments

George H. Rowland[1,2], Katharine R. Hendry[1,3], Amber L. Annett[4], Hong Chin Ng[1], Laura F. Robinson[1,5], Robert M. Sherrell[6], Yuxin Zhou[7], Jerry F. McManus[7], J. Alexander Brearley[3], and Tao Li[1]

[1]School of Earth Sciences, University of Bristol, Bristol, UK, [2]Now at Institute for Marine and Antarctic Studies, University of Tasmania, Hobart, TAS, Australia, [3]British Antarctic Survey, Cambridge, UK, [4]Ocean and Earth Science, University of Southampton, Southampton, UK, [5]Department of Environment and Geography, University of York, York, UK, [6]Department of Marine and Coastal Sciences and Department of Earth and Planetary Sciences, Rutgers University, New Brunswick, NJ, USA, [7]Lamont-Doherty Earth Observatory, Columbia University, Palisades, NY, USA

Key Points:

- Thorium measured in seawater and sediments to quantify glacial trace-element nutrient inputs at the West Greenland margin
- Thorium-232 fluxes are elevated and are similar to other ocean margin sites with high sediment inputs
- Elevated iron fluxes support high primary productivity and reach the beyond the coastal ocean

Supporting Information:

Supporting Information may be found in the online version of this article.

Correspondence to:

G. H. Rowland,
george.rowland@utas.edu.au

Citation:

Rowland, G. H., Hendry, K. R., Annett, A. L., Ng, H. C., Robinson, L. F., Sherrell, R. M., et al. (2025). High lithogenic and micro-nutrient fluxes from the West Greenland margin traced by thorium in seawater and sediments. *Global Biogeochemical Cycles*, *39*, e2025GB008531. https://doi.org/10.1029/2025GB008531

Received 6 FEB 2025
Accepted 15 SEP 2025

Author Contributions:

Conceptualization: George H. Rowland, Katharine R. Hendry, Amber L. Annett, Hong Chin Ng, Laura F. Robinson
Data curation: Katharine R. Hendry, Yuxin Zhou
Formal analysis: George H. Rowland, Katharine R. Hendry, Amber L. Annett, Hong Chin Ng, Laura F. Robinson, Robert M. Sherrell, Yuxin Zhou, Jerry F. McManus, Tao Li
Funding acquisition: Katharine R. Hendry
Investigation: George H. Rowland, Katharine R. Hendry, Amber L. Annett, Hong Chin Ng, Laura F. Robinson, Robert M. Sherrell, Yuxin Zhou, Jerry

Abstract The flux of nutrients from continents to the oceans sustains oceanic primary productivity and is a fundamental component of the carbon cycle. In most regions of the world's oceans primary productivity is limited by the supply of nutrients. In particular, iron can become limiting in the open-ocean due to its low solubility. Glaciated continents have been suggested as an underappreciated source of iron to the high-latitude oceans. Yet, uncertainty remains regarding the magnitude and spatial variability of glacially derived nutrient fluxes, and the extent to which these nutrients impact open-ocean ecosystems. To quantify lithogenic fluxes at the West Greenland margin, we measured ^{232}Th and ^{230}Th in seawater and core-top sediments across the shelf and slope. Our results highlight a negative correlation between low-salinity waters and dissolved and particulate ^{232}Th, suggesting a glacial source for this lithogenic isotope. We calculated dissolved ^{232}Th fluxes 5–24 μg m^{-2} yr^{-1} (100–500 m depth), and sedimentary ^{232}Th fluxes 105–711 μg m^{-2} yr^{-1}, higher than typical open-ocean settings and similar to margin sites influenced by large inputs from aeolian dust and rivers. A sampling transect shows that dissolved ^{232}Th fluxes increase toward Greenland, confirming that lithogenic inputs are sourced laterally from the margin. Using our ^{232}Th fluxes, we estimate an elevated supply of dissolved Fe which extends over the continental slope toward the open ocean. This Fe flux is large enough to support much of the local primary productivity, highlighting the importance of lithogenic fluxes in supporting the marine ecosystem in high-latitude oceans.

Plain Language Summary Small plant-like creatures (algae) living in the surface ocean are an important food source for other marine creatures and affect the Earth's climate by drawing carbon dioxide into the ocean when they grow. In most parts of the oceans the algae's growth is limited because they do not have enough of certain nutrients, such as iron. It is possible that around Greenland, algae are supplied with iron that comes from mud ground-up by ice on the continent. There are no measurements of how much, and how quickly, mud (and iron) reaches the algae in the ocean far away (around 100 km) from the coast of Greenland. We measured two types of the radioactive element thorium in seawater, and seafloor mud, to calculate the rate that mud is supplied to the ocean off West Greenland. We found that high amounts of thorium and iron are supplied to the region, enough to account for the large quantity of algae growing there. This suggests that the ice on Greenland, and maybe also on Antarctica, helps to keep the algae in the ocean growing. Changes to Earth's ice-sheets might then impact how algae grow and absorb carbon dioxide in the future.

1. Introduction

The rate at which carbon is fixed by marine phytoplankton and exported from the surface ocean is a key variable in the global carbon cycle, and is linked to changes in the Earth's climate (Hain et al., 2014; Wilson et al., 2022). One important factor regulating carbon exported to depth (export productivity) is the availability of macro and micronutrients for phytoplankton growth (Moore et al., 2013). In some regions of the ocean, one or more key nutrients may be depleted and thus are considered limiting to primary productivity (Moore et al., 2013).

F. McManus, J. Alexander Brearley, Tao Li
Methodology: George H. Rowland, Hong Chin Ng, Laura F. Robinson, Robert M. Sherrell, Tao Li
Project administration: Katharine R. Hendry
Resources: Katharine R. Hendry, Laura F. Robinson, Robert M. Sherrell, Jerry F. McManus
Supervision: Katharine R. Hendry, Hong Chin Ng, Laura F. Robinson, Jerry F. McManus, J. Alexander Brearley
Visualization: George H. Rowland
Writing – original draft: George H. Rowland
Writing – review & editing: George H. Rowland, Katharine R. Hendry, Amber L. Annett, Hong Chin Ng, Laura F. Robinson, Robert M. Sherrell, Yuxin Zhou, Jerry F. McManus, J. Alexander Brearley, Tao Li

Export production is mainly supported by the cycling of dissolved nutrients to the surface ocean from deeper waters (Moore et al., 2013); however, changing inputs of nutrients from external sources can alter regional and global net primary production and export production (Cotrim da Cunha et al., 2007). In recent years, it has been suggested that nutrient limitation in the high-latitude oceans may be alleviated by nutrients supplied by glaciers and ice sheets (Bhatia et al., 2013; Dinniman et al., 2023; Wadham et al., 2019). High inputs of macro- and micronutrients from the Greenland Ice Sheet have been measured at glacial outflows (Hawkings et al., 2014, 2016), which contain disproportionate concentrations of bioavailable elements compared to other settings (Hawkings et al., 2018; Shoenfelt et al., 2019).

Whether glacially derived nutrients relieve nutrient limitation depends on two key factors. The first is the status of the phytoplankton community with respect to nutrient limitation: additional nutrients will only stimulate new productivity if they include the currently limiting nutrient, or co-limiting nutrients. For example, in regions limited by nitrate (Moore et al., 2013), additional fluxes of Fe or phosphate will not increase primary productivity (unless by the stimulation of nitrogen fixing organisms; von Friesen & Riemann, 2020). Second, waters carrying nutrients from the glacial terminus must be transported to the nutrient-limited regions in the open ocean (Arrigo et al., 2017; Hopwood et al., 2018) before the nutrient load is removed from the water column (e.g., by biological uptake in fjords or settling and flocculation of particles; J. Krause et al., 2021; Ng et al., 2024).

There is evidence of Fe limitation in the Irminger and Iceland basins (Hopwood et al., 2018), and of a deficiency in Fe relative to nitrate in the central Labrador Sea (Tonnard et al., 2020). Conversely, data from the East and West Greenland margins show excess of Fe relative to nitrate (Hopwood et al., 2018; Tonnard et al., 2020), suggesting nitrate is the more limiting nutrient. Silicic acid, rather than Fe, appears to limit diatom growth during the spring bloom across parts of the sub-polar North Atlantic, including at the outlet of Godthåbsfjord, close to Nuuk, Greenland (J. W. Krause et al., 2019). Additionally, it has been suggested that light limitation is important during the late summer and autumn (Oliver et al., 2018). Over the continental shelf and slope near Nuuk, Greenland, recent studies indicate high chlorophyll concentrations and moderately productive diatom communities, despite low dissolved macronutrient concentrations (Hendry et al., 2019; Ng et al., 2024). Similarly, Tonnard et al. (2020) link the depletion of nitrate relative to Fe at the Greenland margins to the strong bloom and high chlorophyll concentrations. These results point towards phytoplankton at the Greenland margins that rely on a substantial supply of nutrients to maintain productivity, and may be limited by macro-, rather than micronutrients. Part of the nutrient supply to high-latitude surface waters may arise from upwelling of deep, nutrient rich, marine waters (Cape et al., 2019; Hopwood et al., 2018), diapycnal mixing (Painter et al., 2014), benthic supply (Ng, Cassarino, et al., 2020) or the export of glacially derived particles (Ng et al., 2024). Seasonal convective mixing is thought to account for the dominant flux of Fe to the surface in the Iceland and Irminger basins (Achterberg et al., 2018; Painter et al., 2014). Similarly, winter mixing can supply nutrients to the surface at the West Greenland margin prior to the spring bloom (Harrison et al., 2013); however, a shallow mixed layer persists from spring through to autumn (Arrigo et al., 2017), in part due to fresh surface waters (Rysgaard et al., 2020). Thus, upwelling is less likely during the summer bloom, when glacial melt waters may be a more important nutrient source (Arrigo et al., 2017).

There is a significant knowledge gap in processes governing the export of glacially derived nutrients to the open ocean (Wadham et al., 2019); some nutrients are expected to behave conservatively during estuarine mixing, while others are highly non-conservative (Hopwood et al., 2020; J. Krause et al., 2021). Removal of Fe across salinity gradients in estuarine environments may be >90% (Poulton & Raiswell, 2002) and similar removal has been observed or assumed in Arctic fjords (Hopwood et al., 2020). Despite the large proportion of dissolved Fe that is removed in fjords, Fe concentrations close to fjord outlets (∼5–10 nM) can still be an order of magnitude larger than those on the surface of nearby coastal (∼<1 nM) or open (∼< 0.5 nM) oceans (Hopwood et al., 2016; J. Krause et al., 2021; Tonnard et al., 2020). Thus, the transfer of waters from fjords to the open ocean may also be associated with a flux of nutrients. In addition to melt waters, Fe sourced from sediment resuspension has been demonstrated in other glaciated coastal settings (Sherrell et al., 2018). Nevertheless, there have been few quantitative assessments of lithogenic fluxes to the open oceans close to ice sheets, and significant uncertainty remains regarding their importance in supplying these nutrients (Hawkings et al., 2020; Hopwood et al., 2015, 2020; Wadham et al., 2019).

Terrigenous fluxes from the Greenland Ice Sheet have been estimated by combining suspended sediment concentrations (from remote sensing) and modeled ice sheet run-off (Overeem et al., 2017). These estimates indicate

a suspended sediment flux of 86 Tg/yr from glaciers near Nuuk, ~60% of which is sourced from the Sermeq Glacier (SG) (Overeem et al., 2017). This is equivalent to ~10% of Amazon River suspended sediment flux (Peucker-Ehrenbrink, 2018) and suggests that terrigenous fluxes toward at the West Greenland margin are appreciable and may be comparable to other regions of high terrigenous flux across the globe. However, sediment deposition in fjords is substantial (Andresen et al., 2024) and the extent to which high suspended sediment fluxes transit fjords and propagate to the ocean is not clear (Overeem et al., 2017).

Here we make a quantitative assessment of the lithogenic supply over the West Greenland continental shelf and slope by applying a scavenging model to measurements of lithogenic ^{232}Th and radiogenic ^{230}Th in seawater and core-top sediments. We extend our quantitative assessment to estimate fluxes of dissolved Fe and argue that our flux estimates represent a plausible lower bound for the region.

2. Materials and Methods

In the following section, we outline the theoretical models, sampling methods and laboratory procedures used in our study. A more detailed description of sampling, laboratory methods and quality control is given in Supporting Information S1.

2.1. Using ^{232}Th/^{230}Th to Calculate Lithogenic Fluxes

2.1.1. Dissolved Thorium Isotopes

The method we use in this study calculates the vertical removal (scavenging) flux of ^{232}Th onto particles, and by assuming steady-state, estimates the supply of ^{232}Th required to balance this removal—assumed to be from dissolving lithogenic particles, analogous to aeolian dust deposition (Hayes et al., 2013; Hsieh et al., 2011). At our study sites, lithogenic material is likely delivered laterally from the continent through surface waters, such that vertical removal fluxes are directly linked to lateral lithogenic supply (Hendry et al., 2019; Supporting Information S1).

To estimate fluxes of dissolved ^{232}Th (d^{232}Th), we calculate the residence time of dissolved thorium by measuring radiogenic dissolved ^{230}Th (d^{230}Th), which is depleted in seawater compared to its parent isotope ^{234}U, due to adsorption onto particles (which subsequently sink, 2.1.2; Bacon & Anderson, 1982). The integrated deficit of d^{230}Th, relative to production by ^{234}U, provides a measure of the ^{230}Th removal rate (Broecker et al., 1973; Hsieh et al., 2011). Assuming a steady state and negligible contributions from advection and eddy diffusion, the scavenging timescale for ^{230}Th is equivalent to a residence time (Equation 1). A vertically integrated removal flux of ^{232}Th can be calculated for different depths by applying the integrated ^{230}Th residence time to ^{232}Th inventories (Hayes et al., 2013, Equation 2). Application of ^{230}Th residence times to ^{232}Th requires an assumption that the isotopes share the same chemical behavior (e.g., speciation), despite their different sources. Though subject to some uncertainty, initial studies testing this assumption suggest that the isotopes share similar speciation (Anderson et al., 2025; Hayes et al., 2017; Hayes, Fitzsimmons, et al., 2015; Pavia, Anderson, Pinedo-Gonzalez, et al., 2020).

This approach has been used to estimate fluxes of ^{232}Th from dust in the open-ocean Atlantic and Pacific (Anderson et al., 2016; Hayes et al., 2013, 2017, 2018; Hayes, Fitzsimmons, et al., 2015; Hsieh et al., 2011; Pavia, Anderson, Winckler, & Fleisher, 2020), as well as in the Southern Ocean to determine glacial lithogenic fluxes (Pérez-Tribouillier et al., 2020). A modeling study indicates that 2/3 of global ^{232}Th input may be linked to a sedimentary source, although ^{232}Th inventories disproportionately reflect surface inputs (Xu & Weber, 2025). For the margin setting investigated here, with dynamic physical oceanography, we also consider the impacts of advection and diffusion on our flux calculations (Supporting Information S1).

In Equation 1 the integration is carried out using the trapezium rule and the activities from surface to the first sample in a depth transect are assumed to be constant (as might be expected in the surface mixed layer). For profiles with the shallowest sample at >50 m (CTD8, 9, and 24), a surface ^{230}Th concentration is estimated from the average of shallow samples from the other profiles (CTD4, 6 and 14; Supporting Information S1) to allow for integration to depth. The low surface concentrations mean that this approximation contributes a small amount to the total ^{230}Th inventory: doubling the estimated surface ^{230}Th concentration increases the inventory at the deepest profile depths by only 2%–5%. In Equation 1, λ_{230} is the decay constant of thorium-230, and ^{230}Th and ^{234}U are the activities of each isotope per volume of seawater. The subscript "xs" refers to ^{230}Th that is not derived

from lithogenic material—estimated using the d^{232}Th concentration and 4×10^{-6} mol/mol as an estimate of ^{230}Th/^{232}Th released from lithogenic particles (within uncertainty of average upper continental crust, UCC, assuming secular equilibrium in the ^{238}U series; Roy-Barman et al., 2009; Rudnick & Gao, 2003). The average fraction of lithogenic ^{230}Th is 16% of the total, but is up to 54% for shallow samples with high ^{232}Th, such that shallow ^{230}Th concentrations are sensitive to the chosen lithogenic ^{230}Th/^{232}Th ratio. Because ^{230}Th profiles are integrated in Equation 1, the sensitivity of our flux calculations to this ratio is reduced. For example, at CTD006, halving the lithogenic ^{230}Th/^{232}Th to 2×10^{-6} mol/mol (the lower uncertainty bound for UCC; Rudnick & Gao, 2003) produces a ~40% decrease in ^{232}Th flux at 5 m depth, but only an 11% decrease at 642 m.

$$\tau_{\mathrm{Th}_z}[\mathrm{yr}] = \frac{\int_0^z {}^{230}\mathrm{Th}_{\mathrm{xs}}\, dz}{\lambda_{230}\int_0^z \left({}^{234}U - {}^{230}\mathrm{Th}_{xs}\right) dz} \tag{1}$$

$${}^{232}\mathrm{Th\ flux}_{\,Z}\left[\mu\mathrm{g\ m^{-2}\ yr^{-1}}\right] = \frac{\int_0^z {}^{232}\mathrm{Th}\, dz}{\tau_{\mathrm{Th}_z}} \tag{2}$$

$$\mathrm{Fe\ flux}\left[\mathrm{mg\ m^{-2}\ yr^{-1}}\right] = {}^{232}\mathrm{Th\ flux} \times \mathrm{UCC}_{\mathrm{Fe/Th}} \times S_{\mathrm{Fe/Th}} \tag{3}$$

The supply of other dissolved trace metals (e.g., Fe) can be assessed using the ratios of abundance (in upper continental crust, $\mathrm{UCC}_{\mathrm{Fe/Th}}$) and solubility relative to ^{232}Th ($S_{\mathrm{Fe/Th}}$; Equation 3; Hayes, Anderson, et al., 2018). For Fe, previous studies either assumed $S_{\mathrm{Fe/Th}} = 1$ or used estimates from leaching mineral dust (Hayes et al., 2017, 2018; Hayes, Fitzsimmons, et al., 2015) and used existing estimates of Fe/Th from the bulk or upper continental crust (Hayes et al., 2013, 2018; Rudnick & Gao, 2003; Taylor & McLennan, 1995).

2.1.2. Thorium-230 Normalization

A related method to estimate lithogenic fluxes in the modern ocean is ^{230}Th normalization applied to core-top sediments (Anderson et al., 2016; Rowland et al., 2017). This technique relies on the assumption that the scavenging removal flux of ^{230}Th on sinking particles is equal to its well-established production rate from ^{234}U (β) in the water column above (Francois et al., 2004). This assumption has been demonstrated to be accurate to within ~30–40% in most of the ocean and the method has been widely applied to modern and Pleistocene sediments (Costa et al., 2020). By combining the ^{230}Th-normalized vertical settling flux of sediment (Equation 4) with the concentration of ^{232}Th in the sediment, a flux of ^{232}Th can be derived for core-top sediments (Equation 5). Our dissolved and sedimentary approaches both compare the well-constrained production of d^{230}Th against its concentration to estimate fluxes (cf. denominator, Equation 1 and numerator, Equation 4). To calculate a mass flux, only ^{230}Th derived from ^{234}U in the overlying water column is considered, $^{230}\mathrm{Th}_{\mathrm{xs}}$; it is necessary to estimate and subtract lithogenic and authigenic ^{234}U from the total. This estimation relies on assumed ratios of lithogenic and authigenic ^{238}U/^{232}Th and ^{230}Th/^{238}U; fluxes are particularly sensitive to the assumed ratios when the proportion of ^{230}Th in these fractions is high (Missiaen et al., 2018). We assess this sensitivity for our sites in the supplementary information (Figure S1 in Supporting Information S1). We correct for ^{230}Th decay since deposition by assuming an age of 1,000 and 2000 years for sediments 0–1 and 1–2 cm depths, respectively. Because core-top ages are likely to be much less than the half-life of ^{230}Th, decay corrections have little effect on calculated mass fluxes; varying the assumed ages from 0 to 5,000 years changes the calculated mass fluxes by <5%.

$$\mathrm{Mass\ flux}\left[\mathrm{g\ m^{-2}\ yr^{-1}}\right] = \frac{\beta\left[\mathrm{dpm\ m^{-3}yr^{-1}}\right] \times z\ [\mathrm{m}]}{{}^{230}\mathrm{Th}_{\mathrm{xs},0}[\ \mathrm{dpm\ g^{-1}}]} \tag{4}$$

$${}^{232}\mathrm{Th\ flux}_{\ \mathrm{Sed}}\left[\mu\mathrm{g\ m^{-2}\ yr^{-1}}\right] = \mathrm{Mass\ flux} \times {}^{232}\mathrm{Th}\left[\mu\mathrm{g\ g^{-1}}\right] \tag{5}$$

2.2. Oceanographic Setting of the West Greenland Margin

Samples were collected at the West Greenland margin in July-August 2017 during the DY081 cruise, onboard the RRS *Discovery* (Hendry et al., 2019). Shallow flow (~<200 m) at the West Greenland margin is dominated by the West Greenland Current (WGC) that flows north-westwards, parallel to the coast, forming part of the sub-polar gyre (Figure 1; Holliday et al., 2007; Myers et al., 2009). During the 2017 DY081 cruise, geostrophic velocities in

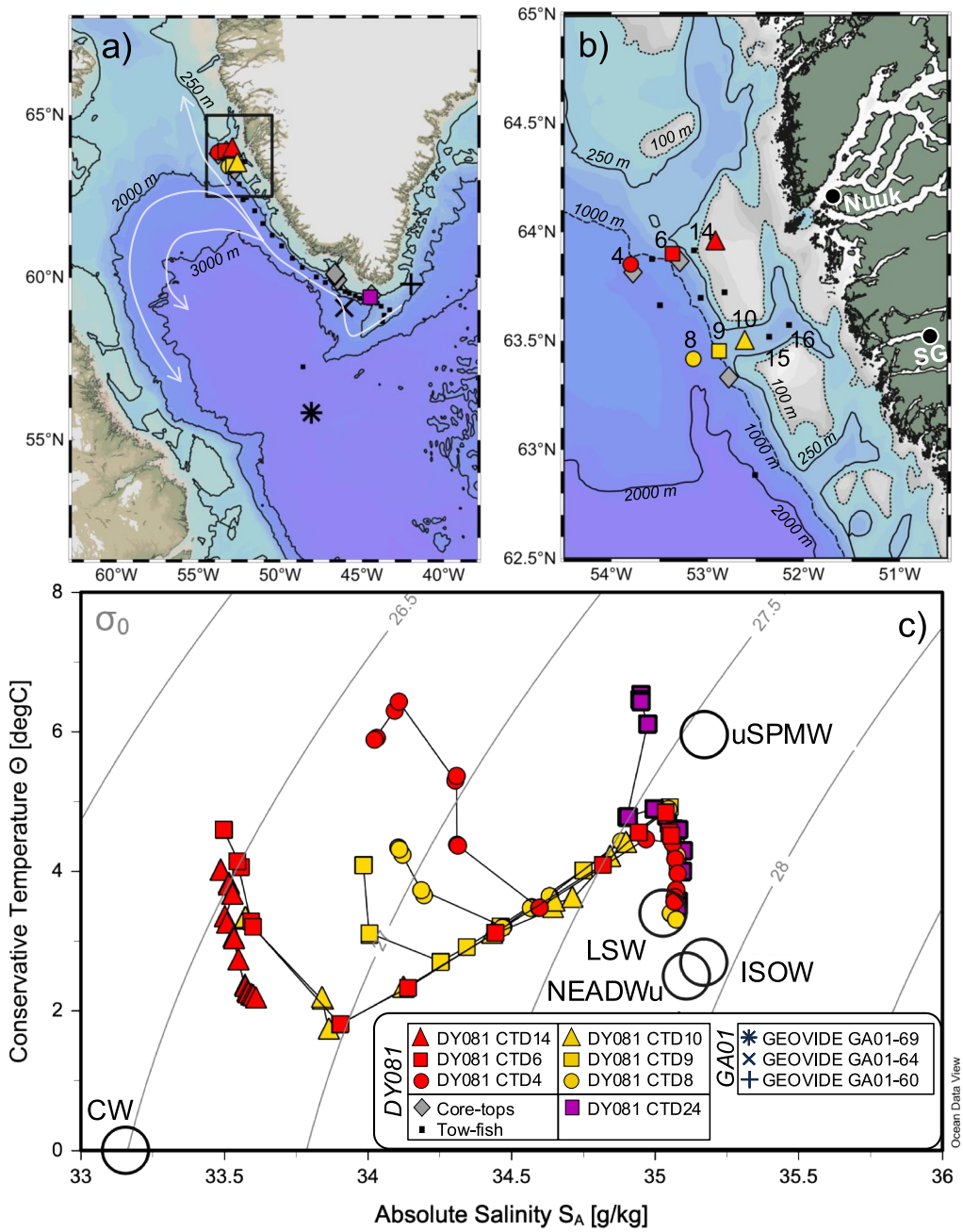

Figure 1. (a) Sample sites at the West Greenland margin during the DY081 cruise (this study, colored symbols) and three sample sites from the GEOVIDE cruise (Deng et al., 2018; large black symbols). Small black squares indicate the location of DY081 underway (tow-fish) surface particulate samples (also shown in Figure 2). White arrows schematically depict surface currents. (b) The sampling grid offshore Nuuk: the location of Nuuk and the Sermeq Glacier (SG) are indicated and bathymetry is shown on a color scale and by black isolines. (c) Hydrography of sampling sites and approximate end-member water-mass compositions (open circles) from the literature: CW = Greenland coastal water, uSPMW = upper sub-polar mode water, LSW = Labrador Sea water, ISOW = Iceland-Scotland overflow water, NEADWu = upper Northeast Atlantic deep water (García-Ibáñez et al., 2018; Rysgaard et al., 2020). Figure created using Ocean Data View (Schlitzer, 2025).

the cores of the WGC were measured to be on the order of 0.1–0.3 m s^{-1} (Hendry et al., 2019). The study area has high eddy kinetic energy (Cuny et al., 2002), and eddies move heat and buoyancy delivered by the boundary currents further into the Labrador Sea interior (Saenko et al., 2014). The hydrography at our sites (Hendry et al., 2019) is controlled by the balance of Greenland coastal water (CW, mostly <50 m), upper sub-polar mode

water (uSPMW, increasing to ~500 m) (Rysgaard et al., 2020), and a contribution from a cooler, slightly saltier, water mass (>500 m, Figure 1). All our sites also show a strong thermocline, with temperatures decreasing from the surface to a depth of ~30–50 m.

Measurements of chlorophyll concentration and biogenic silica (i.e., diatom) productivity during the DY081 cruise (Hendry et al., 2019) indicate there is an active phytoplankton community off West-Greenland. Median biogenic silica productivity in the sampling grid offshore Nuuk (Figure 1b) was >2x the global average (Hendry et al., 2019; Nelson et al., 1995). These initial findings suggest that a relatively high supply of micronutrients (e.g., Fe) may be required to sustain the high levels of productivity, and that as macronutrient concentrations are low in the surface waters, the plankton may be limited by these nutrients.

2.3. DY081 Cruise and Sampling

Samples were collected during the DY081 cruise in July 2017 as part of the wider ICY-LAB project (Isotope CYcling in the LABrador sea; Hendry et al., 2019). Water samples (~5 L, $n = 24$) were collected from 7 CTD casts, southwest of Nuuk (6 casts), and near Cape Farewell (1 cast; Figure 1). Samples were filtered through 0.2 μm pore-size membrane filters and collected in acid-cleaned polypropylene 6 L containers. The samples collected in cast CTD024 were filtered using a 0.45 μm pore-size filter. After filtration, samples were immediately acidified to pH ~2 using ~5 mL of concentrated Romil UpA HCl (Anderson et al., 2012).

Surface particulate trace metal samples were collected at a depth of ~2 m while the ship was moving using a trace-metal clean underway towed-fish apparatus (e.g., Annett et al., 2017). Samples of unfiltered seawater (3 L) were collected in acid-cleaned HDPE bottles and then filtered through acid-cleaned Supor 0.45 μm filters at <34 kPa using filtered air.

Sediment samples were taken from the top (0–1 cm and 1–2 cm intervals) of short (<40 cm) cores collected using a mega (multi)-corer (5 cores, 7 samples) and remotely operated vehicle (9 push-cores, 10 samples), recovered from water depths 953–1,327 m. Cores were sliced into 1 cm intervals during the cruise, and the samples were stored refrigerated prior to analysis.

2.4. Laboratory Procedures

Filtered seawater samples were processed at the University of Bristol in the Bristol Isotope Group clean laboratory broadly following procedures set out by previous studies (Auro et al., 2012; Ng, 2016; Ng, Robinson, et al., 2020; Rowland et al., 2017). The main acids used in the laboratory, HNO_3 and HCl, were distilled in-house using Teflon stills. The other reagents used were Romil SpA grade, and Milli-Q water with a resistivity of 18.2 MΩ cm.

To summarize briefly the laboratory protocol, ~5 L samples were weighed and spiked with known amounts of ^{229}Th and ^{236}U from two separate spike solutions. Thorium and uranium were co-precipitated with $Fe(OH)_3$ by the addition of concentrated ammonium hydroxide. Supernatants were separated from precipitates by a peristaltic pump and the precipitates were collected and dissolved. Uranium and thorium were separated and purified using anion exchange column chromatography. Before analysis, samples were subjected to an oxidative step involving $HClO_4$, H_2O_2 and concentrated HNO_3.

Surface water particulate samples were processed at Rutgers University, according to previously established methods (Annett et al., 2017; Planquette & Sherrell, 2012): filtered particles were fully digested in Teflon containers on a hotplate using a mixture of HNO_3 and HF. Sediment samples were analyzed at Lamont-Doherty Earth Observatory (LDEO) according to previously published methods (Fleisher & Anderson, 1991, 2003). Sediment was spiked with a mixed ^{236}U-^{229}Th spike and digested by heating samples in a mixture of concentrated HNO_3, $HClO_4$ and HF. Uranium and thorium were separated from the sample matrix by co-precipitation with Fe $(OH)_3$ and anion exchange column chromatography. Acids were ACS "Plus grade" and "Optima grade" (Fisher Scientific).

2.5. Mass Spectrometry

Dissolved Th isotopes were analyzed at the University of Bristol by multi-collector inductively coupled plasma mass spectrometry (MC-ICP-MS) following the peak-jumping routine of Auro et al. (2012) and following the

protocols of Ng (2016). Each sample was bracketed by clean acid to monitor and correct the instrumental blank, and also by a thorium bracketing standard to correct for instrument mass bias and the ion counter yield. Corrections were also made for the tailing of the larger ^{232}Th beam on ^{230}Th and ^{229}Th masses. Uncertainties based on the signal variability were propagated through all corrections. The measured ^{230}Th concentration is corrected for the radioactive ingrowth of ^{230}Th from ^{234}U since the time of sample filtration (Anderson et al., 2012; Robinson et al., 2004).

Particulate ^{232}Th surface samples were analyzed at Rutgers University as part of a multi-element method using single-collector high-resolution ICP-MS according to previously established methods (Annett et al., 2017; Planquette & Sherrell, 2012). Concentrations were quantified relative to external standard solutions, and corrected for sensitivity drift and matrix effects using added ^{115}In, and for full procedural blanks. Sedimentary thorium and uranium isotopes were analyzed at LDEO by ICP-MS (Thermo Scientific Element Plus). A uranium standard (SRM129) was used to correct for instrumental mass bias and to determine detector gain. Corrections were also made for the tailing of the larger ^{238}U and ^{232}Th beams on the minor isotopes.

Full procedural blanks (one or two per batch) for dissolved ^{232}Th were 13 ± 16 pg (2σ, $n = 7$), with only one >15 pg and for ^{230}Th were 0.3 ± 0.4 fg (2σ, $n = 7$), with one >0.4 fg. Blank corrections make up a maximum of 4% and 5% of the total analyte mass for ^{232}Th and ^{230}Th respectively. Procedural blanks for particulate ^{232}Th samples were 2.79 ± 1.86 pg, which represents 1%–18% of the signal for samples reported here (mean = 6%). Based on a typical volume filtered of 2–3 L, our detection limit for particulate ^{232}Th in seawater using this method is 3.9–5.9 pg kg^{-1}. One full procedural blank for sediment samples measured at LDEO contained 1.1 ± 0.02 ng ^{232}Th (±2σ) and 40 ± 1.1 fg (±2σ) ^{230}Th, representing <0.6% and <0.4% of the respective analytes.

3. Results

3.1. Surface Particulate ^{232}Th Concentrations

Surface particulate ^{232}Th (p^{232}Th) concentrations show a large range from 10 to 552 pg/kg. High concentrations >300 pg/kg are seen at the Nuuk sampling grid and off Narsaq (~60°N, 47°W) (Figure 2a), where low salinity waters are also present. Two distinct negative correlations exist between p^{232}Th and salinity, specific to longitude ranges, with the relationship for samples collected <50°W showing a shallower gradient than those collected >50°W (closer to Nuuk) (Figure 2c). The two regression lines converge around a salinity of 34 and p^{232}Th concentration of ~75 pg/kg. Concentrations of p^{232}Th are much lower (generally ≤20 pg/kg) at sites with higher salinities and/or further from the coast.

3.2. Dissolved ^{232}Th and ^{230}Th Concentrations

Dissolved ^{232}Th concentrations ranged from 54 to 360 pg/kg, with a mean of 138 ± 86 (1σ). For each CTD cast, the values are highest in the shallowest samples, and decrease from the surface to a mid-depth minimum around 500 m. Results from CTD004 also show small but consistent increases in the 4 samples from ~500 to 1,050 m. Deeper than 500 m, concentrations of ^{232}Th are highest closer to the coast (at a given depth) for both transects at Nuuk. The two transects show a similar range of values. Three samples from CTD024 off the southern tip of Greenland, which were filtered using 0.45 μm filters, have similar values to those collected off Nuuk.

Dissolved ^{230}Th$_{xs}$ concentrations range from 0.9 to 4.5 fg/kg and generally increase with depth from the surface (Figure 3b). Below ~100 m, concentrations increase in a linear fashion, while above 100 m the gradient with depth is steeper as concentrations decrease toward the surface. Two samples measured at the same depth at CTD004 are within 2σ uncertainty of each other. Below ~100 m at the northern Nuuk transect, concentrations are slightly higher offshore (cf. CTD006 and CTD004), while concentrations are invariant with distance from the coast at the southern transect. Concentrations at Cape Farewell (CTD024) are similar to those at Nuuk at the same depths and also increase with depth. Shallower than 100 m the DY081 data are similar to those reported from the GEOVIDE cruise (Deng et al., 2018), around 1–2 fg/kg near the surface, but below 100 m DY081 data are generally lower at equivalent depths, by ~0.5 fg/kg for data near Cape Farewell and by >1 fg/kg for stations in the central Labrador sea (Deng et al., 2018; Moran et al., 1997, 2002).

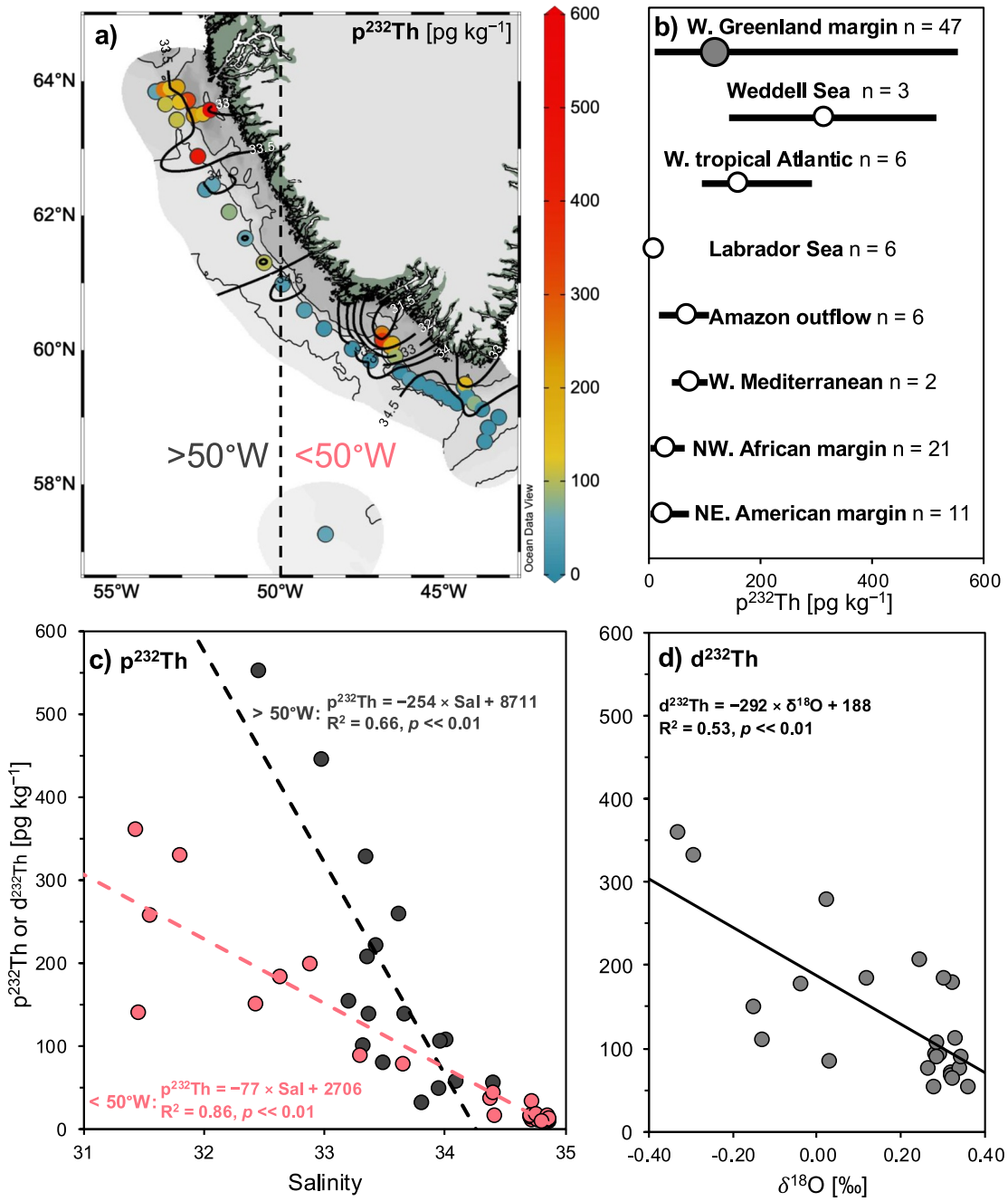

Figure 2. (a) Surface concentration of $p^{232}Th$ (pg kg^{-1}) is shown on the color scale. Black contours show the average salinity of underway samples. (b) Compilation of $p^{232}Th$ concentrations (<500 m depth): symbols = average, bars = range and n = number of samples. Data are from: the Weddell Sea (Venchiarutti et al., 2011); the western tropical Atlantic (station 2; Hayes et al., 2017); the Labrador Sea and near the Amazon outflow (Moran et al., 2002); the western Mediterranean (Gdaniec et al., 2018); the northwest African and northeast American margins (Hayes et al., 2018). (c) Correlations between salinity and $p^{232}Th$ for surface underway samples: black symbols > 50°W; red symbols < 50°W. (d) Correlation between dissolved ^{232}Th concentrations (all depths, pg kg^{-1}) and $\delta^{18}O$ (‰). Probability values (p) for gradients of regression slopes are based on a two-tailed t-test. Panel (a) created using Ocean Data View (Rafter, 2025; Schlitzer, 2025).

3.3. Thorium-230-Derived Residence Times and Dissolved ^{232}Th Fluxes

Residence times of thorium (τ_{Th}) range from 1.6 to 6 years, and generally increase with depth from the surface, although the shallowest three data points from CTD004 show a reversal of this trend in the top 50 m (Figure 3). The three sites in the northern Nuuk transect show a spread in τ_{Th} at <100 m, with values converging below this depth.

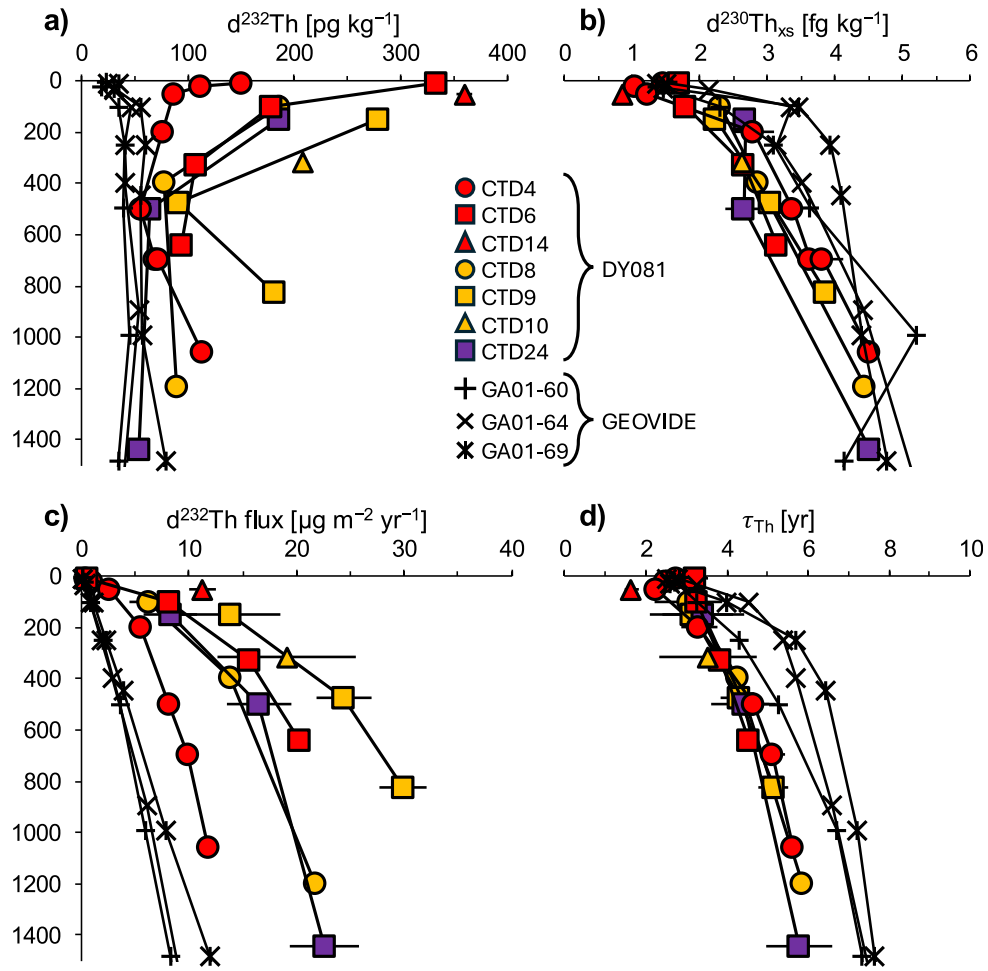

Figure 3. Concentrations (a), (b) of dissolved ^{232}Th and ^{230}Th$_{xs}$, integrated ^{232}Th flux (c) and ^{230}Th residence time (d) near Nuuk and Cape Farewell during the DY081 cruise. The deepest samples from each profile are within 30 m of the seafloor except for CTDs 8 and -9 (deepest samples 486 and 489 m above the seafloor). Data from the GEOVIDE cruise (black symbols, Deng et al., 2018) are also shown; only GEOVIDE data within the depth range of DY081 samples are shown. Residence times and ^{232}Th fluxes from GEOVIDE data (Deng et al., 2018) are calculated assuming ^{238}U = 3.15 ng/g and ^{234}U/^{238}U activity ratio of 1.147.

Integrated fluxes of d^{232}Th increase sharply with depth and range from 0.3 to 10 μg m^{-2} yr^{-1} in the surface 50 m and 8–30 μg m^{-2} yr^{-1} at depths >300 m (Figure 3). Fluxes at different CTD sites converge toward the surface and diverge at greater depths, with steeper gradients with depth in the upper 500 m. At both Nuuk transects, fluxes are generally higher closer to the coast. Fluxes from CTD024 (Cape Farewell) lie within the range of fluxes at Nuuk.

3.4. Sedimentary ^{230}Th and ^{232}Th Concentrations and ^{230}Th-Normalized Fluxes

Thorium-232 concentrations in core-top sediments range from 3.48 to 10.76 μg g^{-1}, (average 4.91 ± 1.74, 1σ), indicating that a substantial portion of the sediment is lithogenic (upper continental crust ~10.5 μg g^{-1}; Rudnick & Gao, 2003). Total ^{230}Th (activity) concentrations ranged from 0.56 to 1.44 dpm g^{-1}. Due to the large lithogenic fraction and shallow water depth of the sample sites, the proportions of unsupported ^{230}Th (^{230}Th$_{xs}$) are low and sensitive to the assumed values of ^{238}U/^{232}Th and ^{230}Th/^{238}U in lithogenic material. Applying our best estimates of lithogenic ^{238}U/^{232}Th and ^{230}Th/^{238}U ratios (activity ratios of 0.45 and 0.816 respectively) gives ^{230}Th$_{xs}$ concentrations from 0 to 1.04 dpm g^{-1}, which corresponds to ^{230}Th normalized mass fluxes of 23–120 g m^{-2} yr^{-1}, and ^{232}Th fluxes 105–711 μg m^{-2} yr^{-1} (ignoring ^{230}Th$_{xs}$ values within error of zero). The range of ^{232}Th fluxes changes to 91–412 μg m^{-2} yr^{-1} (^{238}U/^{232}Th = 0.3; ^{230}Th/^{238}U = 0.75) and 133–944 μg m^{-2} yr^{-1} (^{238}U/^{232}Th = 0.6; ^{230}Th/^{238}U = 0.95) when changing the lithogenic correction factors. Our choice of lithogenic

correction factors and the sensitivity of ^{232}Th fluxes is detailed in the (Figure S1 and Table S1 in Supporting Information S1). We note that the uncertainty introduced to ^{232}Th fluxes by chosen lithogenic ratios will likely be systematic for a given location because the sediments are of similar age and share a similar lithogenic source. Because of this uncertainty, we interpret the range of ^{232}Th fluxes calculated across our multiple sampling sites.

4. Discussion

4.1. High Lithogenic Signals Linked to Glacial Waters

The spatial pattern of surface water p^{232}Th concentrations (Figure 2a) highlights key areas of very high lithogenic particulate load at the Greenland margin. As might be expected, the (>0.45 μm) particulate concentrations are greater than those observed in the open ocean (e.g., Moran et al., 1997) and show that large amounts of lithogenic particles reach the waters overlying the continental shelf and slope. The association of high p^{232}Th with low-salinity surface waters suggests a strong link between glacially derived waters and particulate lithogenic material, and suggests a sufficiently long residence time for lithogenic particles to maintain quasi-conservative behavior in the shelf-slope region surface waters (Figure 2c). This behavior is consistent with the rapid transport of fjord-derived particles across the shelf (Figure S2 in Supporting Information S1). The glacial origin of the low salinity waters is further supported by a strong correlation between δ^{18}O and salinity in surface waters (0–10 m; $R^2 = 0.95$; Hendry et al., 2019). This association between glacially derived waters and high lithogenic contents is also supported by the d^{232}Th data, with moderate correlations between δ^{18}O (and salinity) and d^{232}Th concentrations across all sample depths (Figure 2d).

It is possible that the relationship between freshwater tracers and ^{232}Th is a distal signal advected from the Arctic or East Greenland in the boundary current system. However, we observed two distinct relationships between salinity and p^{232}Th at our sampling locations, which suggests that more localized processes may alter the lithogenic loading per unit freshwater in different source regions/catchments (e.g., differences in glaciation style, geomorphology, lithology, particle removal rates and hydrography of fjord systems). The steeper gradient for samples >50°W (Figure 2c) implies a higher relative lithogenic content for meltwaters derived from around Nuuk than from the sites further south and east. This result is consistent with a recent study that calculated that the outlet from SG into Sermilik fjord (Figure 1b), (~50 km from our highest p^{232}Th concentration site), is thought to contribute ~25% of the suspended sediment flux from the entire Greenland ice sheet (Overeem et al., 2017). Indeed, satellite images show plumes of material emanating from the fjords toward our sampling sites (Figure S2 in Supporting Information S1), sometimes crossing the shelf within ~2 days (Supporting Information S1). Such rapid transport of particles across the shelf could explain how the different p^{232}Th versus salinity correlations are maintained, despite the strong boundary current (i.e., the transport time in the WGC for ~680 km between Cape Farewell and the sampling grid at Nuuk at 0.35 m/s is ~26 days).

Local variations in geology may also influence the amount of ^{232}Th exported from a catchment. Stream sediments enriched in lanthanum (with which Th correlates; Rudnick & Gao, 2003; Steenfelt, 2012) and U/Th mineralization (Armour-Brown et al., 1983) both argue for elevated ^{232}Th in source lithologies around Southern Greenland (i.e., closer to our sites <50°W). Likewise, younger rocks around the southern tip of Greenland may have higher ^{232}Th concentrations than Archaean rocks dominant in the area around Nuuk (Henriksen et al., 2009; Taylor & McLennan, 1995). Therefore, lithological influences probably act to reduce p^{232}Th concentrations at sites >50°W; higher sediment inputs (Overeem et al., 2017) must outweigh these factors to produce the steeper relationship between p^{232}Th and salinity at these sites.

Resuspension of sediment at the ocean floor can elevate dissolved and particulate ^{232}Th concentrations in the water column (Hayes et al., 2018; Schlitzer et al., 2018). Elevated turbidity is measured at ~170 m and 350–460 m, toward the head of the Nuuk trough (CTD16 and -15; Figures 1b, Figure S6 in Supporting Information S1), but this signal is not seen at our sample locations further offshore (CTD8, -9, -10), or at the northern Nuuk transect (CTD4, -6, -14; Figure 1). We are therefore confident that the majority of particulate ^{232}Th is supplied at or near the surface. The shallow maxima in d^{232}Th concentrations are also consistent with a major source at the surface. However, there are hints of a moderate subsurface shelf/slope source of d^{232}Th at CTD4 and -9, where ^{232}Th concentrations increase below ~500 m (Figure 3). It is possible that d^{232}Th sourced from sediment resuspension (or released from pore-waters during resuspension; Cochran et al., 1986) could be transported along isopycnals toward CTD08 and -09, explaining some of the elevation of d^{232}Th toward the surface at those sites.

4.2. Lithogenic Signals at the Greenland Margin in a Global Context

4.2.1. Dissolved and Particulate ^{232}Th Concentrations

The highest DY081 p^{232}Th concentrations from close to Nuuk and Narsaq are an order of magnitude, or more, higher than surface open ocean measurements from the Labrador Sea (Figure 2b; Moran et al., 1997, 2002). The average surface p^{232}Th concentration oceanward of the 1,000 m isobath at Nuuk, ~88 pg/kg, is high compared to previous surface measurements in the central Labrador Sea, ~10 pg/kg (Moran et al., 2002). Compared to other regions with high lithogenic input, DY081 surface p^{232}Th concentrations are still considerable (Figure 2b). For example, in the western tropical Atlantic, close to the Amazon outflow, concentrations are 62–108 pg/kg (Moran et al., 2002) and in the western Mediterranean are up to 106 pg/kg at 100 m, although <50 pg/kg in general (filtered onto 1 μm filters; Gdaniec et al., 2018). At the east Atlantic margin p^{232}Th concentrations are <20 pg/kg (at depths <200 m in the 0.8–51 μm size fraction), while those at the northwest Atlantic margin offshore North America are up to ~70 pg/kg (Hayes et al., 2018). Close to the West Antarctic Peninsula, similarly high p^{232}Th concentrations, up to ~300 pg/kg, have been measured in waters ~200 m (Venchiarutti et al., 2011).

The DY081 d^{232}Th concentrations are also high compared to the east Atlantic margin, up to 175 pg/kg, under the influence of high fluxes of Saharan dust (<50 m depth; Hayes, Anderson, et al., 2018) and as high as surface waters influenced by both dust and river inputs, up to ~230 pg/kg, from the western tropical Atlantic (Hayes et al., 2017). Close to the glaciated West Antarctic peninsula, d^{232}Th concentrations are 100–110 pg/kg at their subsurface maximum ~150–180 m water depth (Venchiarutti et al., 2011). The evidence, therefore, from both dissolved and particulate ^{232}Th concentrations suggests a strong contribution of lithogenic material to seawater chemistry at the Greenland margin, comparable to other areas of high lithogenic inputs. This observation is consistent with satellite data, indicating a high input of suspended sediment from glacial outflows (Overeem et al., 2017) and importantly suggests that elevated lithogenic loads are not completely trapped in fjord systems.

The GEOVIDE sites GA01-60 and −64 (Deng et al., 2018), are ~70–100 km offshore (Figure 1), oceanward of the 1,500 m isobath off the southern tip of Greenland, and show much lower surface d^{232}Th surface concentrations, suggesting that waters with high lithogenic content may be confined quite close to the shelf around Cape Farewell. Differences in ^{232}Th depth profiles moving offshore are also seen between the West Antarctic Peninsula and Drake Passage (Venchiarutti et al., 2011) and such differences between open-ocean and margin ^{232}Th profiles have also been predicted by modeling due to water mass exchange (Roy-Barman, 2009). The convergence of some GEOVIDE and DY081 ^{232}Th concentrations below ~500 m (e.g., CTD24) indicates that either scavenging or water-mass exchange may reduce the spatial differences at these greater depths.

4.2.2. Dissolved ^{232}Th Fluxes

The calculated ^{232}Th scavenging fluxes indicate a strong source of lithogenic material derived from the continent (Figure 3). Compared to vertical fluxes calculated from the data of Deng et al. (2018) around Cape Farewell and the central Labrador Sea (GEOVIDE cruise), DY081 data are elevated at all depths except the top ~50 m, where the fluxes converge. Below ~200 m the DY081 fluxes are up to ~3x higher (at equivalent depths) than those typically observed in the open ocean, (<5.5 μg m^{-2} yr^{-1} in the South Atlantic and North Pacific; Deng et al., 2014; Hayes et al., 2013) (Figure 4a). This is not unexpected for a continental margin setting, but simply demonstrates that scavenged ^{232}Th fluxes at the West Greenland margin are indeed elevated and that the region is influenced by a horizontal supply of glacially derived lithogenic trace-metals that extends into the Labrador Sea, and is not confined to fjords only (Hopwood et al., 2015). Furthermore, ^{232}Th fluxes at the West Greenland margin are comparable to, or higher than, those observed at continental margins influenced by some of the world's largest lithogenic sources: Saharan dust and the Amazon and Orinoco Rivers (Figures 4a and 4c; Hayes et al., 2017; Hayes, Anderson, et al., 2018). The depth-trend in ^{232}Th fluxes is probably a result of a violation of one or more of the scavenging model assumptions (Supporting Information S1); explaining these trends is a topic of active research and although there is no consensus on an optimum integration depth, most studies consider depths ~50–500 m for estimating dust inputs (Anderson et al., 2016; Deng et al., 2014; Hayes et al., 2013, 2017; Pavia, Anderson, Winckler, & Fleisher, 2020). We present full ^{232}Th flux depth profiles for comparison to the literature, but expect fluxes at depths <100 m to be more severely impacted by violations of model assumptions (Supporting Information S1) and so consider a set range of integration depths in our discussion of Fe supply (Section 4.3.1).

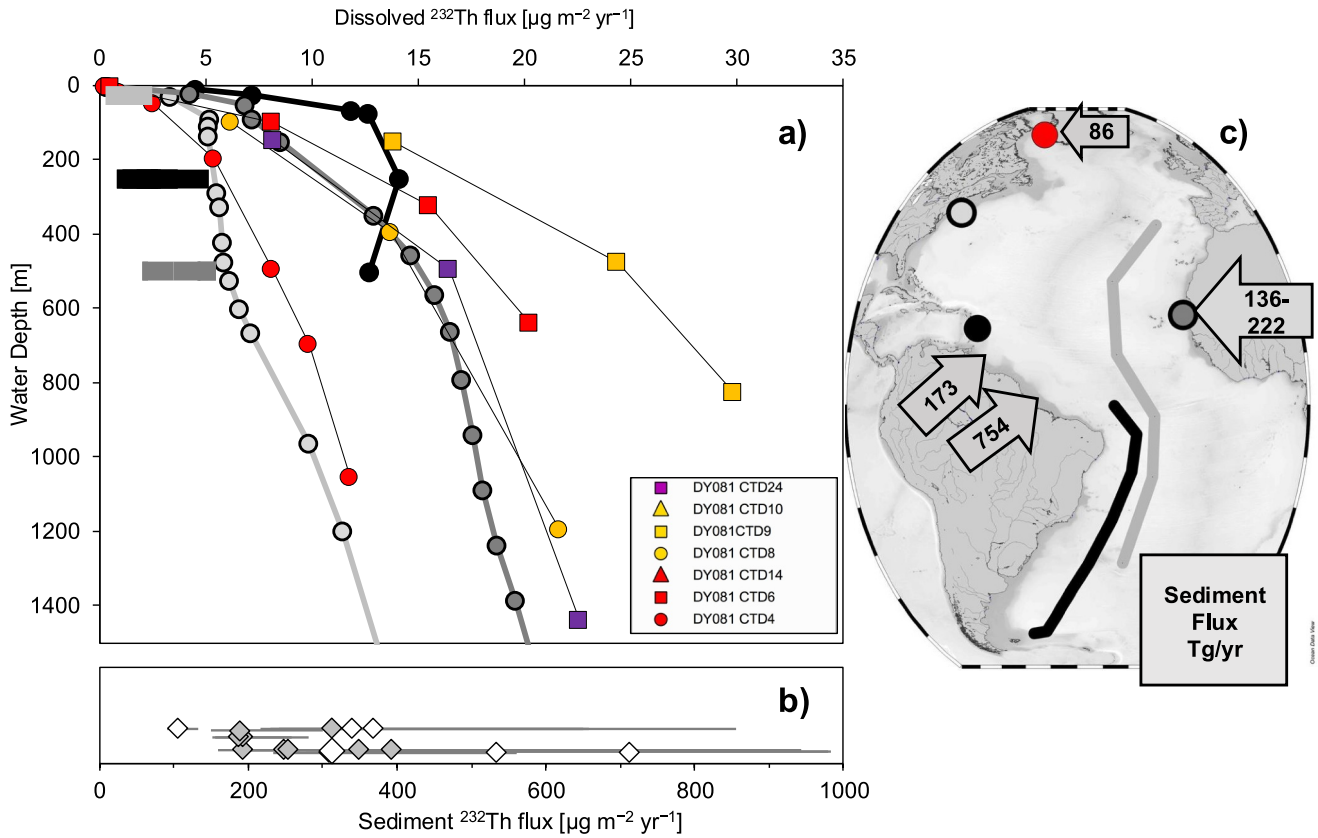

Figure 4. (a) Dissolved ^{232}Th fluxes (thin lines) and (b) core-top sediment ^{232}Th fluxes using ^{238}U/^{232}Th = 0.45, ^{230}Th/^{238}U = 0.816 (diamonds: gray = Southwest Greenland, white = Nuuk; distributed vertically for clarity) from the West Greenland margin. Dissolved ^{232}Th fluxes (a) from near the North America (light gray), Africa (dark gray), South America (black) are also shown (greyscale circles, thick lines; Hayes et al., 2017; Hayes, Anderson, et al., 2015, Hayes et al., 2018). Open-ocean ^{232}Th fluxes at fixed integration depths are shown (solid bars) from the Atlantic (25 m light gray, Hsieh et al., 2011; 250 m black, Deng et al., 2014) and North Pacific (500 m, dark gray, Hayes et al., 2013, not shown on map). The map shows the compiled sites from the Atlantic with estimates of terrigenous sediment input from the Amazon and Orinoco rivers (Peucker-Ehrenbrink, 2018), Saharan dust (Yu et al., 2019) and glacial sediment input around Nuuk (Overeem et al., 2017) in Tg/yr. Error bars on sediment ^{232}Th fluxes indicate the range of fluxes by varying lithogenic activity ratios between ^{238}U/^{232}Th = 0.3–0.6 and ^{230}Th/^{238}U = 0.75–0.95 while keeping ^{230}Th$_{xs}$ > 0 (the full range of possible sediment ^{232}Th fluxes is shown in Figure S1 in Supporting Information S1). Dissolved Fe fluxes estimated in this study are directly proportional to ^{232}Th fluxes (for $S_{Fe/Th}$ = 1 and Fe/Th = 3,271 g/g: Fe/^{232}Th ~ 3.3 mg/μg ~ 60 μmol/μg. For $S_{Fe/Th}$ = 0.4: ~1.3 mg/μg ~ 23 μmol/μg).

The increased proximity of DY081 sites to the continent compared with the literature sites (~40–50 vs. ~200 km at West African margin) could partly explain higher ^{232}Th values. A second line of evidence for elevated lithogenic fluxes at our sites comes from core-top sediments, with average total ^{232}Th fluxes, 312 ± 148 μg m^{-2} yr^{-1}, (≥2x late-Holocene ^{230}Th-normalized ^{232}Th fluxes at the South American and African margins; Rowland et al., 2021). Multiplying the average total ^{232}Th fluxes by an estimate of S_{Th}~3–5% (Baker et al., 2020; Hayes et al., 2013) gives dissolved fluxes similar to our scavenging estimates at ~500 m (i.e., ~10–15 μg m^{-2} yr^{-1}). A further check on our flux estimates can be made using the suspended sediment flux estimated for glaciers around Nuuk from satellite data (Overeem et al., 2017). Assuming an exponential decrease in flux with distance, we estimate ~1% of the suspended sediment flux from glaciers could reach our sites (Text S4 in Supporting Information S1), giving a total possible ^{232}Th flux of ~9.2 × 10^6 g ^{232}Th/yr. Distributing this flux over a square 100^2–150^2 km^2 around our sites suggests a total potential vertical ^{232}Th flux of ~410–920 μg m^{-2} yr^{-1}, generally higher than our core-top ^{232}Th fluxes (Supporting Information S1).

4.2.3. Do Physical Transports Lead to Overestimates of d^{232}Th Supply?

The vertical gradients of ^{230}Th and ^{232}Th in the upper ~250 m will act to transport ^{230}Th into the surface layer, and ^{232}Th out of the layer, leading to underestimates of ^{232}Th removal fluxes in each case (Supporting Information S1). Boundary scavenging near ocean margins (Anderson et al., 1983) may also mean that our dissolved and

sedimentary ^{232}Th fluxes are too low (e.g., only ~70% of their true values; Costa et al., 2020; Hayes, Fleisher, et al., 2015).

The strong near-surface ^{232}Th gradient across the shelf and strong currents at our sites could introduce additional terms to ^{232}Th mass balance that are not accounted for by our model. Near Nuuk we calculate a potential advective supply of ^{232}Th in the upper 50 m across the shelf that is >10x larger (~380 μg m^{-2} yr^{-1}) than our highest scavenging removal fluxes (Supporting Information S1). Although we expect much of this supply to be removed along the shelf by the WGC (Supporting Information S1), the size of the potential advective supply implies that total ^{232}Th supply at our sites could be larger than we estimate from scavenging removal alone, and is possibly dominated by advection instead of particle dissolution (Supporting Information S1).

Such large advective fluxes imply short ^{232}Th residence times, raising the possibility that measured ^{232}Th concentrations are not at steady state, but could represent a more transient elevation (e.g., due to input from fjords during the melt season). In such a scenario, scavenging removal fluxes would be overestimates of the long-term mean. However, given the additional ^{232}Th potentially supplied by advection, and the agreement with our estimates calculated using alternative methods (4.2.2), we consider it unlikely our scavenging based fluxes overestimate the total ^{232}Th supply.

4.3. Fe Fluxes and Biological Requirements

4.3.1. Fe Fluxes at the West Greenland Margin and Globally

The vertical removal flux of d^{232}Th has been used to estimate dissolved Fe fluxes across a range of oceanographic settings including the tropical Pacific, western tropical Atlantic and across the North Atlantic (Hayes et al., 2013, 2017, 2018; Hayes, Fitzsimmons, et al., 2015). These studies have mainly focused on assessing aeolian supply to open ocean areas. The approach assumes that Fe and ^{232}Th are both supplied predominantly from the dissolution of lithogenic material at a fixed ratio such that variation in Th inputs scale with Fe supply (i.e., it is assumed that no sources exist that supply Th without associated Fe, and vice versa).

In our glacial margin setting the source of ^{232}Th is dissolution of lithogenic material, so we assume an Fe/Th ratio of 3,271 g/g, a composition typical for the upper continental crust (Hayes, Fitzsimmons, et al., 2015; Taylor & McLennan, 1995). For the area around Nuuk, the presence of dominant Archaean rocks (Henriksen et al., 2009) means that the ratio may be substantially larger (>10^4 g/g; Taylor & McLennan, 1995), making our Fe fluxes conservative for this region. The ratio of Fe:Th fractional solubility ($S_{Fe/Th}$) was estimated to be 1 by earlier studies (Hayes, Fitzsimmons, et al., 2015), but more recent leaching experiments on Saharan dust imply that Fe and Th are not released congruently, suggesting a wider range of $S_{Fe/Th}$ (0.4–1.3; Hayes, Anderson, et al., 2018). Independent of the $S_{Fe/Th}$ and Fe/Th values, our iron fluxes represent a lower bound as they are derived from ^{232}Th fluxes that are likely underestimated due to the local hydrography (Supporting Information S1).

The average dissolved Fe flux across all sites ranged from 16 to 52 mg m^{-2} yr^{-1} for solubility ratios of 0.4 and 1.3, respectively (279–906 μmol m^{-2} yr^{-1}; Table S2 in Supporting Information S1). As the Fe fluxes are proportional to ^{232}Th fluxes they share the same spatial patterns and comparison to other global sites in Figure 4 (Figure S5 in Supporting Information S1). Due to violations in scavenging-model assumptions at shallow depths (Supporting Information S1; Pavia, Anderson, Winckler, & Fleisher, 2020), we consider Fe fluxes at greater integration depths (100–200 and 200–500 m) to give better estimates (Table S2 in Supporting Information S1; Figure 5). Considering these depths, our lower bound for iron fluxes at the West Greenland margin is comparable to those found in other high lithogenic input settings (Figure 4; Table S2 in Supporting Information S1), such as near the Amazon River (Hayes et al., 2017) or under the Saharan dust plume (Hayes et al., 2018).

If supplies of Fe and Th become decoupled before reaching our study sites, for example, if Fe is released from sediments due to reductive dissolution (Tonnard et al., 2020), then this method will underestimate the fluxes of Fe. Despite these uncertainties, our flux estimates provide the first quantitative constraints on the supply of Fe from dissolving lithogenic particles at the West Greenland margin. As lithogenic particles are supplied laterally (Figure 2), our Fe flux estimates constrain the horizontal Fe supply that must balance the vertical removal from West Greenland.

We also make an additional estimate of dissolved Fe supply based on our core-top ^{232}Th fluxes and an estimate of fractional Fe solubility (S_{Fe}). We estimate S_{Fe} as 2.55%, from the average of two Alaskan glacial flour samples

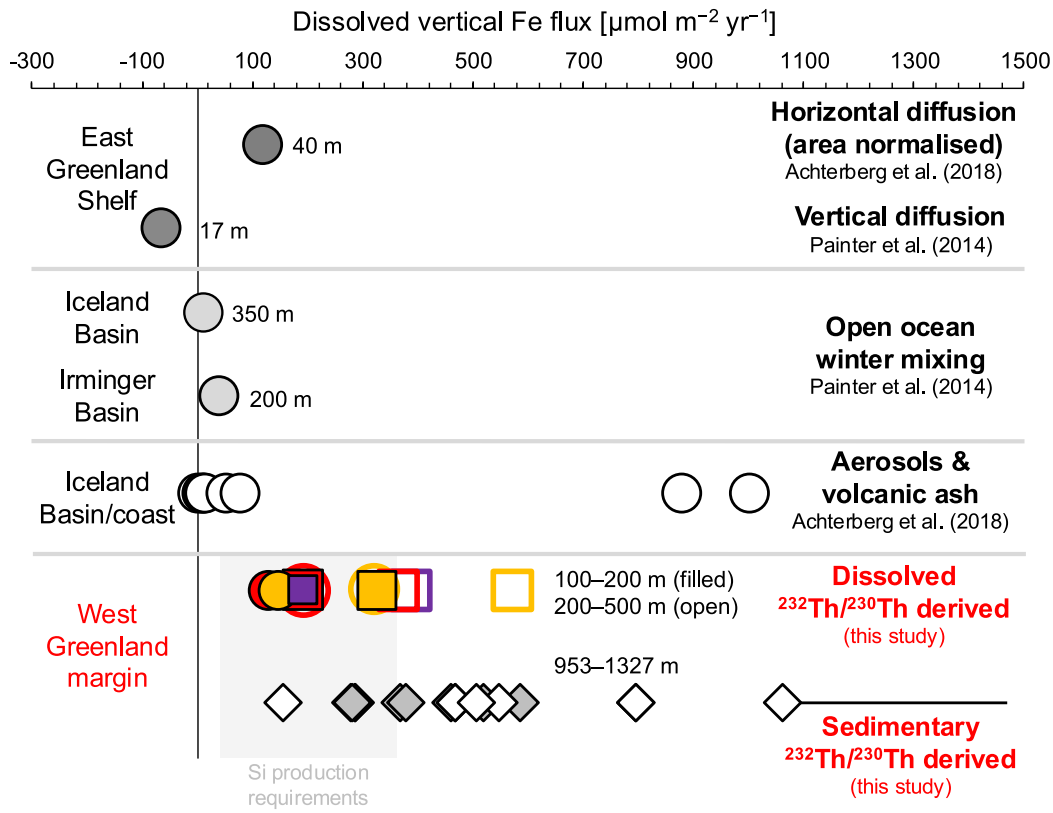

Figure 5. Estimated dissolved Fe vertical fluxes in the high-latitude North Atlantic from different sources. Fe flux estimates from dissolved ^{232}Th/^{230}Th are calculated for depths 100–200 m (filled symbols) and 200–500 m (open symbols) using $S_{Fe/Th}$ = 0.4 and Fe/Th = 3,271 g/g. Dissolved Fe flux estimates derived from core-top sediment ^{232}Th/^{230}Th for Nuuk (white diamonds) and Southwest Greenland (gray diamonds) were calculated using S_{Fe} = 2.55% and Fe/Th = 3,271 g/g, and lithogenic activity ratios ^{238}U/^{232}Th = 0.45 and ^{230}Th/^{238}U = 0.81. Error bars show fluxes when estimated with ^{238}U/^{232}Th = 0.3–0.6 and ^{230}Th/^{238}U = 0.75–0.81 (the error bar for the lowest flux is smaller than the symbol size). The possible range of Fe demand by siliceous primary producers is indicated by a gray shaded region (main text, Section 4.3.2). Horizontal fluxes at the East Greenland shelf were normalized to an approximate shelf-area in the original study (Achterberg et al., 2018). Negative fluxes indicate net Fe removal. The highest Fe fluxes from aerosols include direct input from a volcanic eruption during Spring 2010 (Achterberg et al., 2018). Water depths over which fluxes are calculated or integrated are shown.

(Schroth et al., 2009). Although the S_{Fe} estimate is based on samples from a different location, primary Fe(II) silicates contribute most of the Fe in both the Alaskan and DY081 sediments (Fe(II)/total Fe ~35–80%; Shoenfelt et al., 2019); this likely exerts a strong influence on Fe solubility (Hawkings et al., 2018). Our dissolved Fe flux estimates based on these assumptions and core-top data range from 156 to 1,062 μmol m^{-2} yr^{-1} (average 466 ± 222 μmol m^{-2} yr^{-1}, 1σ), consistent with significantly elevated Fe fluxes at our sites (Figure 5).

4.3.2. Do Physical Transports Bias Fe Supply Estimates?

Because the supply of ^{232}Th could be dominated by advection (4.2.3), rather than particle dissolution, it is possible that the supply of Fe and Th become decoupled along the advection pathway (Hayes et al., 2018), and our model overestimates Fe supply (Equation 3). However, because the potential advective ^{232}Th flux is ~10x our supply estimate based on scavenging removal fluxes, our estimates of Fe supply would remain conservative unless iron was removed relative to Th by the same factor (i.e., >~10x).

Dissolved Fe and Th are both expected to be strongly removed across salinity gradients in fjords; data from the Baltic Sea (for Th) and the fjords around Nuuk (for Fe) indicate this removal process occurs at a similar salinity for both elements (~10–15) (Andersson et al., 1995; Hopwood et al., 2016), with concentrations decreasing by a factor of 18 (Fe) and 28 (Th). Additionally, in particle-rich coastal and estuarine environments, Fe and Th have been shown to have very similar short residence times of ~1–20 days, suggesting rapid removal of both elements

at similar rates (McKee, 2008; Santschi et al., 1980; Shen et al., 2024). Thus, it seems unlikely that the large lateral advective flux of $d^{232}Th$ (or Fe) could be supported by the direct export of $d^{232}Th$ and Fe from fjords, and that the elements would not be expected to fractionate strongly even in such a scenario. Instead, the very high concentrations of $p^{232}Th$ and the high ^{232}Th fluxes measured in core-top sediments both suggest the dissolution of lithogenic particles as an important supply term for ^{232}Th (and Fe) at our sites.

4.3.3. Fe Supply and Uptake at Nuuk

The Fe fluxes presented in this study are comparable to, or higher than, other sites situated in areas of high lithogenic inputs measured using the same methods (e.g., the Amazon river and dust inputs; Hayes et al., 2017; Figure 4). This supports the notion that fluxes of lithogenic material from Greenland are globally significant (Overeem et al., 2017) and are likely to be of importance in supplying lithogenic nutrients at least on a regional scale. It is likely, given its continuously glaciated nature, that the rest of the margin supplies lithogenic nutrients to the ocean, though inputs at the western margin are expected to be the largest (Overeem et al., 2017). However, the relative importance of a given flux of Fe in terms of biogeochemistry is determined by the requirements of phytoplankton in the local area. During the DY081 cruise, biogenic silica production was estimated using incubation experiments (Hendry et al., 2019) to be ~2–14 mmol m^{-2} day^{-1} around Nuuk. These estimates made during summer may well represent an upper estimate for the annual productivity at these sites (due to favorable conditions for diatom growth), but they can be used to assess the importance of the Fe fluxes calculated here to a first approximation.

Using typical diatom molar uptake ratios of Si:C ~ 0.13 (Brzezinski, 2004) and C:Fe ~ 10^5 as estimated by Tagliabue and Arrigo (2005) for diatoms in the Ross Sea (which is also at high latitude, surrounded by glaciated continental margins and likely has high Fe input) we can then estimate the Fe supply required by diatoms around Nuuk to sustain the measured biogenic silica production. Although this approach has caveats, including the poorly constrained stoichiometry of nutrient uptake by diatoms—which is dependent on the degree of Fe stress amongst other factors (Hutchins & Bruland, 1998; Koch & Trimborn, 2019)—our calculations allow a first approximation of the Fe requirements of diatoms at our sample sites.

Scaling up the measured Si productivity to an annual productivity estimate gives a range of Fe supply required by diatoms around Nuuk of ~60–400 μmol m^{-2} yr^{-1} (3–22 mg m^{-2} yr^{-1}), which, the large uncertainties notwithstanding, overlaps the range of average estimates of Fe flux calculated here. Assuming a shorter, perhaps more realistic, growing season length of ~8 months at our sites (Arrigo et al., 2017) indicates required Fe fluxes of ~40–260 μmol m^{-2} yr^{-1}. The supply of dissolved Fe from the lithogenic material is thus likely to contribute a dominant proportion of the Fe required for diatom growth at Nuuk, even when considering the lower value of $S_{Fe/Th}$ (Figure 5). Additional supply of Fe due to upwelling or due to diapycnal diffusivity is also possible; however, upwelling can be suppressed during the spring and summer due to stronger stratification (Arrigo et al., 2017; Oliver et al., 2018), and the dominant wind directions are seldom favorable for upwelling (Hopwood et al., 2015). Vertical diffusivity has been shown to supply only small amounts of Fe to the surface mixed layer in the Irminger basin (Achterberg et al., 2018), and leads to removal of Fe at the East Greenland shelf (Painter et al., 2014). Deeper mixing supplying dissolved Fe from greater depths may become more important during the winter (Achterberg et al., 2018). Thus, the flux of Fe from the dissolution of lithogenic material seems likely to account for the most important supply term. This conclusion is supported by the fact that our chosen values for $UCC_{Fe/Th}$ and $S_{Fe/Th}$ (Figure 5) and the effects of lateral and vertical diffusion (Supporting Information S1) mean that our Fe estimates probably represent a lower bound.

4.3.4. Regional Context of Fe Supply

Our aim is to assess whether lithogenic fluxes are particularly elevated at the Greenland margin, so that we choose values for $UCC_{Fe/Th}$ and $S_{Fe/Th}$ that are conservative with respect to the Fe flux magnitude, allowing us to provide a lower bound on these fluxes for our sites.

A previous study calculated and compiled Fe fluxes to surface waters in the Irminger and Iceland basins from a range of processes, including aeolian deposition, horizontal supply from shelves, vertical mixing and diapycnal diffusivity (Achterberg et al., 2018). A horizontal Fe flux estimate for the East Greenland shelf—converted to a vertical flux equivalent by Achterberg et al. by normalizing to a surface area—is 117 μmol m^{-2} yr^{-1}, lower than our vertical Fe fluxes estimated for the West Greenland margin (>128 μmol m^{-2} yr^{-1} for $S_{Fe/Th} = 0.4$; Table S2 in

Supporting Information S1; Figure 5). The dissolved Fe fluxes we reconstruct for the West Greenland margin from sediments and seawater are higher than the other fluxes calculated or compiled by Achterberg et al., except for the input of Fe-rich ash from a volcanic eruption (Figure 5). This finding highlights the potential significance of the large glacially derived lithogenic supply to the nearby coastal ocean.

Achterberg et al. concluded that the large fluxes measured at the East Greenland shelf could not propagate into the basin interior (i.e., limited to <100 km) due to strong density gradients in the East Greenland current. For our sites on the west Greenland margin, isopycnals are inclined downwards toward the continental slope and flatten at shallower depths toward the open ocean hundreds of kilometers offshore (Lee, 2007; Sarthou et al., 2018; Figure S6 in Supporting Information S1). Combined with high horizontal eddy diffusivity in the region, the density structure could provide a mechanism for the mixing of sub-surface margin waters (i.e., ∼100–300 m), with a strong lithogenic imprint, toward the surface waters of the interior of the Labrador sea (Funk et al., 2009; Kawasaki & Hasumi, 2014; Figure S6a in Supporting Information S1). Thus, the Fe fluxes at the West Greenland Margin may be more significant in supplying Fe to the open-ocean Labrador Sea than holds for the equivalent setting on the East Greenland Margin for the Irminger basin. Likewise, GEOVIDE cruise results show elevated particulate Fe concentrations and fluxes off the West Greenland margin compared with the eastern margin (Gourain et al., 2019; Lemaitre et al., 2020).

5. Conclusion and Outlook

In this study, we have presented some of the first estimates of lithogenic fluxes to the ocean at the West Greenland margin. Concentrations of the isotope ^{232}Th suggest that a significant lithogenic source accompanying low-salinity melt waters is transported offshore from Nuuk; concentrations of both p^{232}Th and d^{232}Th are as high or higher than at other sites with high lithogenic input. Using measurements of ^{232}Th/^{230}Th in filtered seawater and sediments, we show that vertical ^{232}Th fluxes in our study region are high, though not unprecedented, when compared with other continental margins. Our dissolved ^{232}Th fluxes, although likely to be underestimates (Supporting Information S1), are much higher than those in the open-ocean, and the elevated ^{232}Th concentrations and fluxes reach oceanward of the 1,000 m isobath. These results confirm that the Greenland margin, and possibly glaciated margins more generally, do act as important sources of lithogenic material (including micronutrients) to the ocean, and that the estuarine process in fjords does not completely remove the high glacial inputs at these sites (Arrigo et al., 2017; Bhatia et al., 2013; Hopwood et al., 2015, 2020). Our core-top ^{230}Th-normalized ^{232}Th fluxes also provide a modern reference point for studies of changing glacial lithogenic fluxes through the late Pleistocene (e.g., Zhou & McManus, 2024).

Our ^{232}Th/^{230}Th data suggest that fluxes of Fe at the West Greenland margin are higher than those at the East Greenland shelf (Achterberg et al., 2018). We calculated that the Fe fluxes from lithogenic inputs are probably large enough to support all of the silica productivity measured during the DY081 cruise, confirming that glacially derived lithogenic material can be important for sustaining primary productivity in the region (Ng et al., 2024). We suggest that high lithogenic inputs combine with local hydrography to advect the signals toward the basin interior, potentially supplying lithogenic nutrients off the shelf to primary producers in the Labrador Sea. Thus, our results support the more general hypothesis that glacially derived lithogenic nutrients do supply open-ocean ecosystems (Hawkings et al., 2020; Wadham et al., 2019).

The application of our method in a setting with very dynamic physical oceanography means our estimates would benefit from comparison to future independent estimates, such as sediment traps or ^{230}Th-normalization of filtered particles (Anderson et al., 2016). These kinds of supporting data may become available in the future as the high-latitude oceans and glaciated continental margins remain in focus as key areas of global change.

Conflict of Interest

The authors declare no conflicts of interest relevant to this study.

Data Availability Statement

All the data on which this study is based can be found in Rowland (2025) and Hendry et al. (2024).

Acknowledgments
We thank the captain, crew, technicians and science team of *RRS Discovery* expedition DY081 for facilitating a successful field campaign. We thank Christopher D. Coath for assistance with the mass spectrometry in Bristol. GHR was supported by a NERC DTP studentship (NE/L002434/1). KRH was supported by European Research Council starting grant ICY-LAB (grant agreement 678371). The contribution of JFM was supported in part by the US-NSF. We thank two anonymous reviewers whose comments helped to improve the manuscript.

References

Achterberg, E. P., Steigenberger, S., Marsay, C. M., LeMoigne, F. A. C., Painter, S. C., Baker, A. R., et al. (2018). Iron biogeochemistry in the high latitude north Atlantic Ocean. *Scientific Reports*, *8*(1), 1283. https://doi.org/10.1038/s41598-018-19472-1

Anderson, R. F., Bacon, M. P., & Brewer, P. G. (1983). Removal of 230Th and 231Pa at ocean margins. *Earth and Planetary Science Letters*, *66*, 73–90. https://doi.org/10.1016/0012-821X(83)90127-9

Anderson, R. F., Cheng, H., Edwards, R. L., Fleisher, M. Q., Hayes, C. T., Huang, K.-F. F., et al. (2016). How well can we quantify dust deposition to the ocean? *Philosophical Transactions of the Royal Society A: Mathematical, Physical and Engineering Sciences*, *374*(2081), 20150285. https://doi.org/10.1098/rsta.2015.0285

Anderson, R. F., Fleisher, M. Q., Robinson, L. F., Edwards, R. L., Hoff, J. A., Moran, S. B., et al. (2012). GEOTRACES intercalibration of 230 Th, 232 Th, 231 Pa, and prospects for 10 Be. *Limnology and Oceanography: Methods*, *10*(4), 179–213. https://doi.org/10.4319/lom.2012.10.179

Anderson, R. F., Marcantonio, F., & Pinedo-González, P. (2025). Chemical tracers of scavenging, particle dynamics, and sedimentation processes. In *Treatise on geochemistry* (pp. 479–512). Elsevier. https://doi.org/10.1016/B978-0-323-99762-1.00045-0

Andersson, P. S., Wasserburg, G. J., Chen, J. H., Papanastassiou, D. A., & Ingri, J. (1995). 238U/234U and 232Th/230Th in the Baltic Sea and in river water. *Earth and Planetary Science Letters*, *130*, 217–234.

Andresen, C. S., Karlsson, N. B., Straneo, F., Schmidt, S., Andersen, T. J., Eidam, E. F., et al. (2024). Sediment discharge from Greenland's marine-terminating glaciers is linked with surface melt. *Nature Communications*, *15*(1), 1–10. https://doi.org/10.1038/s41467-024-45694-1

Annett, A. L., Fitzsimmons, J. N., Séguret, M. J. M., Lagerström, M., Meredith, M. P., Schofield, O., & Sherrell, R. M. (2017). Controls on dissolved and particulate iron distributions in surface waters of the Western Antarctic Peninsula shelf. *Marine Chemistry*, *196*, 81–97. https://doi.org/10.1016/J.MARCHEM.2017.06.004

Armour-Brown, A., Steenfelt, A., & Kunzendorf, H. (1983). Uranium districts defined by reconnaissance geochemistry in South Greenland. *Journal of Geochemical Exploration*, *19*(1–3), 127–145. https://doi.org/10.1016/0375-6742(83)90013-4

Arrigo, K. R., van Dijken, G. L., Castelao, R. M., Luo, H., Rennermalm, Å. K., Tedesco, M., et al. (2017). Melting glaciers stimulate large summer phytoplankton blooms in southwest Greenland waters. *Geophysical Research Letters*, *44*(12), 6278–6285. https://doi.org/10.1002/2017GL073583

Auro, M. E., Robinson, L. F., Burke, A., Bradtmiller, L. I., Fleisher, M. Q., & Anderson, R. F. (2012). Improvements to 232-thorium, 230-thorium, and 231-protactinium analysis in seawater arising from GEOTRACES intercalibration. *Limnology and Oceanography: Methods*, *10*(7), 464–474. https://doi.org/10.4319/lom.2012.10.464

Bacon, M. P., & Anderson, R. F. (1982). Distribution of thorium isotopes between dissolved and particulate forms in the deep sea. *Journal of Geophysical Research*, *87*(C3), 2045–2056. https://doi.org/10.1029/jc087ic03p02045

Baker, A. R., Li, M., & Chance, R. (2020). Trace metal fractional solubility in size-segregated aerosols from the tropical Eastern Atlantic Ocean. *Global Biogeochemical Cycles*, *34*(6), e2019GB006510. https://doi.org/10.1029/2019GB006510

Bhatia, M. P., Kujawinski, E. B., Das, S. B., Breier, C. F., Henderson, P. B., & Charette, M. A. (2013). Greenland meltwater as a significant and potentially bioavailable source of iron to the ocean. *Nature Geoscience*, *6*(4), 274–278. https://doi.org/10.1038/ngeo1746

Broecker, W. S., Kaufman, A., & Trier, R. M. (1973). The residence time of thorium in surface sea water and its implications regarding the rate of reactive pollutants. *Earth and Planetary Science Letters*, *20*(1), 35–44. https://doi.org/10.1016/0012-821X(73)90137-4

Brzezinski, M. A. (2004). The Si:C:N ratio of marine diatoms: Interspecific variability and the effect of some environmental variables. *Journal of Phycology*, *21*(3), 347–357. https://doi.org/10.1111/j.0022-3646.1985.00347.x

Cape, M. R., Straneo, F., Beaird, N., Bundy, R. M., & Charette, M. A. (2019). Nutrient release to oceans from buoyancy-driven upwelling at Greenland tidewater glaciers. *Nature Geoscience*, *12*(1), 34–39. https://doi.org/10.1038/s41561-018-0268-4

Cochran, J. K. K., Carey, A. E., Sholkovitz, E. R., & Surprenant, L. D. (1986). The geochemistry of uranium and thorium in coastal marine sediments and sediment pore waters. *Geochimica et Cosmochimica Acta*, *50*(5), 663–680. https://doi.org/10.1016/0016-7037(86)90344-3

Costa, K. M., Hayes, C. T., Anderson, R. F., Pavia, F. J., Bausch, A., Deng, F., et al. (2020). 230 Th normalization: New insights on an essential tool for quantifying sedimentary fluxes in the modern and Quaternary Ocean. *Paleoceanography and Paleoclimatology*, *35*(2), e2019PA003820. https://doi.org/10.1029/2019PA003820

Cotrim da Cunha, L., Buitenhuis, E. T., Le Quéré, C., Giraud, X., & Ludwig, W. (2007). Potential impact of changes in river nutrient supply on global ocean biogeochemistry. *Global Biogeochemical Cycles*, *21*(4). https://doi.org/10.1029/2006GB002718

Cuny, J., Rhines, P. B., Niiler, P. P., & Bacon, S. (2002). Labrador Sea boundary currents and the fate of the Irminger Sea water. *Journal of Physical Oceanography*, *32*(2), 627–647. https://doi.org/10.1175/1520-0485(2002)032<0627:LSBCAT>2.0.CO;2

Deng, F., Henderson, G. M., Castrillejo, M., Perez, F. F., & Steinfeldt, R. (2018). Evolution of 231Pa and 230Th in overflow waters of the North Atlantic. *Biogeosciences*, *15*(23), 7299–7313. https://doi.org/10.5194/bg-15-7299-2018

Deng, F., Thomas, A. L., Rijkenberg, M. J. A., & Henderson, G. M. (2014). Controls on seawater 231Pa, 230Th and 232Th concentrations along the flow paths of deep waters in the Southwest Atlantic. *Earth and Planetary Science Letters*, *390*, 93–102. https://doi.org/10.1016/j.epsl.2013.12.038

Dinniman, M. S., St-Laurent, P., Arrigo, K. R., Hofmann, E. E., & van Dijken, G. L. (2023). Sensitivity of the relationship between antarctic ice shelves and iron supply to projected changes in the atmospheric forcing. *Journal of Geophysical Research: Oceans*, *128*(2), e2022JC019210. https://doi.org/10.1029/2022JC019210

Fleisher, M. Q., & Anderson, R. (1991). Particulate matter digestion (from MG to 10's of G) and radionuclide blanks. In D. C. Hurd & D. W. Spencer (Eds.), *Geophysical monograph series* (pp. 221–222). American Geophysical Union. https://doi.org/10.1029/GM063p0221

Fleisher, M. Q., & Anderson, R. F. (2003). Assessing the collection efficiency of Ross Sea sediment traps using 230Th and 231Pa. *Deep-Sea Research Part II Topical Studies in Oceanography*, *50*(3–4), 693–712. https://doi.org/10.1016/S0967-0645(02)00591-X

Francois, R., Frank, M., Rutgers van der Loeff, M. M., & Bacon, M. P. (2004). 230Th normalization: An essential tool for interpreting sedimentary fluxes during the late Quaternary. *Paleoceanography*, *19*(1), PA1018. https://doi.org/10.1029/2003PA000939

Funk, A., Brandt, P., & Fischer, T. (2009). Eddy diffusivities estimated from observations in the Labrador Sea. *Journal of Geophysical Research*, *114*(C4), 4001. https://doi.org/10.1029/2008JC005098

García-Ibáñez, M. I., Pérez, F. F., Lherminier, P., Zunino, P., Mercier, H., & Tréguer, P. (2018). Water mass distributions and transports for the 2014 GEOVIDE cruise in the North Atlantic. *Biogeosciences*, *15*(7), 2075–2090. https://doi.org/10.5194/bg-15-2075-2018

Gdaniec, S., Roy-Barman, M., Foliot, L., Thil, F., Dapoigny, A., Burckel, P., et al. (2018). Thorium and protactinium isotopes as tracers of marine particle fluxes and deep water circulation in the Mediterranean Sea. *Marine Chemistry*, *199*, 12–23. https://doi.org/10.1016/J.MARCHEM.2017.12.002

Gourain, A., Planquette, H., Cheize, M., Lemaitre, N., Menzel Barraqueta, J.-L., Shelley, R., et al. (2019). Inputs and processes affecting the distribution of particulate iron in the North Atlantic along the GEOVIDE (GEOTRACES GA01) section. *Biogeosciences*, *16*(7), 1563–1582. https://doi.org/10.5194/bg-16-1563-2019

Hain, M. P., Sigman, D. M., & Haug, G. H. (2014). The Biological Pump in the Past. In *Treatise on Geochemistry* (2nd ed., Vol. 8, pp. 485–517). Elsevier. https://doi.org/10.1016/B978-0-08-095975-7.00618-5

Harrison, W. G., Yngve Børsheim, K., Li, W. K. W., Maillet, G. L., Sakshaug, E., Skogen, M. D., & Yeats, P. A. (2013). Phytoplankton production and growth regulation in the Subarctic North Atlantic: A comparative study of the Labrador Sea-Labrador/Newfoundland shelves and Barents/Norwegian/Greenland seas and shelves. *Progress in Oceanography*, *114*, 26–45. https://doi.org/10.1016/J.POCEAN.2013.05.003

Hawkings, J. R., Benning, L. G., Raiswell, R., Kaulich, B., Araki, T., Abyaneh, M., et al. (2018). Biolabile ferrous iron bearing nanoparticles in glacial sediments. *Earth and Planetary Science Letters*, *493*, 92–101. https://doi.org/10.1016/J.EPSL.2018.04.022

Hawkings, J. R., Jemma, W., Martyn, T., Jon, T., Elizabeth, B., Alexander, B., et al. (2016). The Greenland Ice Sheet as a hot spot of phosphorus weathering and export in the Arctic. *Global Biogeochemical Cycles*, *30*(2), 191–210. https://doi.org/10.1002/2015GB005237

Hawkings, J. R., Skidmore, M. L., Wadham, J. L., Priscu, J. C., Morton, P. L., Hatton, J. E., et al. (2020). Enhanced trace element mobilization by Earth's ice sheets. *Proceedings of the National Academy of Sciences of the United States of America*, *117*(50), 31648–31659. https://doi.org/10.1073/pnas.2014378117

Hawkings, J. R., Wadham, J. L., Tranter, M., Raiswell, R., Benning, L. G., Statham, P. J., et al. (2014). Ice sheets as a significant source of highly reactive nanoparticulate iron to the oceans. *Nature Communications*, *5*(1), 3929. https://doi.org/10.1038/ncomms4929

Hayes, C. T., Anderson, R. F., Cheng, H., Conway, T. M., Edwards, R. L., Fleisher, M. Q., et al. (2018). Replacement times of a spectrum of elements in the North Atlantic based on thorium supply. *Global Biogeochemical Cycles*, *32*(9), 1294–1311. https://doi.org/10.1029/2017GB005839

Hayes, C. T., Anderson, R. F., Fleisher, M. Q., Serno, S., Winckler, G., & Gersonde, R. (2013). Quantifying lithogenic inputs to the North Pacific Ocean using the long-lived thorium isotopes. *Earth and Planetary Science Letters*, *383*, 16–25. https://doi.org/10.1016/j.epsl.2013.09.025

Hayes, C. T., Anderson, R. F., Fleisher, M. Q., Vivancos, S. M., Lam, P. J., Ohnemus, D. C., et al. (2015a). Intensity of Th and Pa scavenging partitioned by particle chemistry in the North Atlantic Ocean. *Marine Chemistry*, *170*, 49–60. https://doi.org/10.1016/j.marchem.2015.01.006

Hayes, C. T., Fitzsimmons, J. N., Boyle, E. A., McGee, D., Anderson, R. F., Weisend, R., & Morton, P. L. (2015b). Thorium isotopes tracing the iron cycle at the Hawaii Ocean Time-series Station ALOHA. *Geochimica et Cosmochimica Acta*, *169*, 1–16. https://doi.org/10.1016/j.gca.2015.07.019

Hayes, C. T., Fleisher, M. Q., Huang, K.-F., Robinson, L. F., Lu, Y., Cheng, H., et al. (2015c). 230Th and 231Pa on GEOTRACES GA03, the U.S. GEOTRACES North Atlantic transect, and implications for modern and paleoceanographic chemical fluxes. *Deep Sea Research Part II: Topical Studies in Oceanography*, *116*, 29–41. https://doi.org/10.1016/j.dsr2.2014.07.007

Hayes, C. T., Rosen, J., McGee, D., & Boyle, E. A. (2017). Thorium distributions in high- and low-dust regions and the significance for iron supply. *Global Biogeochemical Cycles*, *31*(2), 328–347. https://doi.org/10.1002/2016GB005511

Hendry, K. R., Huvenne, V. A. I., Robinson, L. F., Annett, A., Badger, M., Jacobel, A. W., et al. (2019). The biogeochemical impact of glacial meltwater from Southwest Greenland. *Progress in Oceanography*, *176*, 102126. https://doi.org/10.1016/J.POCEAN.2019.102126

Hendry, K. R., Ng, H. C., & Krause, J. W. (2024). North Atlantic seawater bottle data collected from CTD during RRS Discovery cruise DY081, extended version [Dataset]. *PANGAEA*. https://doi.org/10.1594/PANGAEA.967168

Henriksen, N., Higgins, A. K., Kalsbeek, F., & Pulvertaft, T. C. R. (2009). Greenland from Archaean to Quaternary Descriptive Text to the 1995 Geological map of Greenland 1:2 500 000 2nd Edition. *Geological Survey of Denmark and Greenland Bulletin*, *18*(18), 1–126. https://doi.org/10.34194/geusb.v18.4993

Holliday, N. P., Meyer, A., Bacon, S., Alderson, S. G., & de Cuevas, B. (2007). Retroflection of part of the east Greenland current at Cape Farewell. *Geophysical Research Letters*, *34*(7), L07609. https://doi.org/10.1029/2006GL029085

Hopwood, M. J., Bacon, S., Arendt, K., Connelly, D. P., & Statham, P. J. (2015). Glacial meltwater from Greenland is not likely to be an important source of Fe to the North Atlantic. *Biogeochemistry*, *124*(1–3), 1–11. https://doi.org/10.1007/s10533-015-0091-6

Hopwood, M. J., Carroll, D., Browning, T. J., Meire, L., Mortensen, J., Krisch, S., & Achterberg, E. P. (2018). Non-linear response of summertime marine productivity to increased meltwater discharge around Greenland. *Nature Communications*, *9*(1), 3256. https://doi.org/10.1038/s41467-018-05488-8

Hopwood, M. J., Carroll, D., Dunse, T., Hodson, A., Holding, J. M., Iriarte, J. L., et al. (2020). How does glacier discharge affect marine biogeochemistry and primary production in the Arctic? *The Cryosphere*, *14*(4), 1347–1383. https://doi.org/10.5194/tc-14-1347-2020

Hopwood, M. J., Connelly, D. P., Arendt, K. E., Juul-Pedersen, T., Stinchcombe, M. C., Meire, L., et al. (2016). Seasonal changes in Fe along a glaciated Greenlandic fjord. *Frontiers in Earth Science*, *4*, 15. https://doi.org/10.3389/feart.2016.00015

Hsieh, Y.-T. T., Henderson, G. M., & Thomas, A. L. (2011). Combining seawater 232Th and 230Th concentrations to determine dust fluxes to the surface ocean. *Earth and Planetary Science Letters*, *312*(3–4), 280–290. https://doi.org/10.1016/j.epsl.2011.10.022

Hutchins, D. A., & Bruland, K. W. (1998). Iron-limited diatom growth and Si:N uptake ratios in a coastal upwelling regime. *Nature*, *393*(6685), 561–564. https://doi.org/10.1038/31203

Kawasaki, T., & Hasumi, H. (2014). Effect of freshwater from the West Greenland Current on the winter deep convection in the Labrador Sea. *Ocean Modelling*, *75*, 51–64. https://doi.org/10.1016/J.OCEMOD.2014.01.003

Koch, F., & Trimborn, S. (2019). Limitation by Fe, Zn, Co, and B12 results in similar physiological responses in two antarctic Phytoplankton species. *Frontiers in Marine Science*, *6*, 514. https://doi.org/10.3389/fmars.2019.00514

Krause, J., Hopwood, M. J., Höfer, J., Krisch, S., Achterberg, E. P., Alarcón, E., et al. (2021). Trace element (Fe, Co, Ni and Cu) dynamics across the salinity gradient in Arctic and antarctic Glacier fjords. *Frontiers in Earth Science*, *9*, 725279. https://doi.org/10.3389/feart.2021.725279

Krause, J. W., Schulz, I. K., Rowe, K. A., Dobbins, W., Winding, M. H. S., Sejr, M. K., et al. (2019). Silicic acid limitation drives bloom termination and potential carbon sequestration in an Arctic bloom. *Scientific Reports*, *9*(1), 8149. https://doi.org/10.1038/s41598-019-44587-4

Lee, C. (2007). CTD data from cruise KN192-02 (2020, Februrary 2, exchange version) [Dataset]. *CCHDO Hydrographic Data Archive*. https://doi.org/10.6075/J0CCHDT8

Lemaitre, N., Ne Planquette, H., Dehairs, F., Frédé, F., Planchon, F., Sarthou, G. G., et al. (2020). Particulate trace element export in the North Atlantic (GEOTRACES GA01 transect, GEOVIDE cruise). *ACS Earth and Space Chemistry*, *4*(11), 2185–2204. https://doi.org/10.1021/acsearthspacechem.0c00045

McKee, B. A. (2008). U- and Th-Series Nuclides in Estuarine Environments. In *Radioactivity in the environment* (Vol. 13, pp. 193–225). https://doi.org/10.1016/S1569-4860(07)00006-X

Missiaen, L., Pichat, S., Waelbroeck, C., Douville, E., Bordier, L., Dapoigny, A., et al. (2018). Downcore variations of sedimentary detrital (238U/232Th) ratio: Implications on the use of 230Thxs and 231Paxs to reconstruct sediment flux and Ocean circulation. *Geochemistry, Geophysics, Geosystems*, *19*(8), 2560–2573. https://doi.org/10.1029/2017GC007410

Moore, C. M., Mills, M. M., Arrigo, K. R., Berman-Frank, I., Bopp, L., Boyd, P. W., et al. (2013). Processes and patterns of oceanic nutrient limitation. *Nature Geoscience*, *6*(9), 701–710. https://doi.org/10.1038/ngeo1765

Moran, S. B., Charette, M. A., Hoff, J. A., Edwards, R. L., & Landing, W. M. (1997). Distribution of 230Th in the Labrador Sea and its relation to ventilation. *Earth and Planetary Science Letters*, *150*(1–2), 151–160. https://doi.org/10.1016/s0012-821x(97)00081-2

Moran, S. B., Shen, C.-C., Edmonds, H. N. N., Weinstein, S. E. E., Smith, J. N. N., & Edwards, R. L. L. (2002). Dissolved and particulate 231Pa and 230Th in the Atlantic Ocean: Constraints on intermediate/deep water age, boundary scavenging, and 231Pa/230Th fractionation. *Earth and Planetary Science Letters*, *203*(3–4), 999–1014. https://doi.org/10.1016/S0012-821X(02)00928-7

Myers, P. G., Donnelly, C., & Ribergaard, M. H. (2009). Structure and variability of the West Greenland Current in Summer derived from 6 repeat standard sections. *Progress in Oceanography*, *80*(1–2), 93–112. https://doi.org/10.1016/J.POCEAN.2008.12.003

Nelson, D. M., Tréguer, P., Brzezinski, M. A., Leynaert, A., & Quéguiner, B. (1995). Production and dissolution of biogenic silica in the ocean: Revised global estimates, comparison with regional data and relationship to biogenic sedimentation. *Global Biogeochemical Cycles*, *9*(3), 359–372. https://doi.org/10.1029/95GB01070

Ng, H. C. (2016). *Investigation of sedimentary 231Pa/230Th as a proxy of Atlantic Meridional Overturning Circulation rate and its deglacial application (Doctoral dissertation)*. University of Bristol.

Ng, H. C., Cassarino, L., Pickering, R. A., Woodward, E. M. S., Hammond, S. J., & Hendry, K. R. (2020a). Sediment efflux of silicon on the Greenland margin and implications for the marine silicon cycle. *Earth and Planetary Science Letters*, *529*, 115877. https://doi.org/10.1016/J.EPSL.2019.115877

Ng, H. C., Hendry, K. R., Ward, R., Woodward, E. M. S., Leng, M. J., Pickering, R. A., & Krause, J. W. (2024). Detrital input sustains diatom production off a glaciated Arctic Coast. *Geophysical Research Letters*, *51*(12), e2024GL108324. https://doi.org/10.1029/2024GL108324

Ng, H. C., Robinson, L. F., Rowland, G. H., Chen, S. S., & McManus, J. F. (2020b). Coupled analysis of seawater and sedimentary 231Pa/230Th in the tropical Atlantic. *Marine Chemistry*, *227*, 103894. https://doi.org/10.1016/j.marchem.2020.103894

Oliver, H., Luo, H., Castelao, R. M., van Dijken, G. L., Mattingly, K. S., Rosen, J. J., et al. (2018). Exploring the potential impact of Greenland meltwater on stratification, photosynthetically active radiation, and primary production in the Labrador Sea. *Journal of Geophysical Research: Oceans*, *123*(4), 2570–2591. https://doi.org/10.1002/2018JC013802

Overeem, I., Hudson, B. D., Syvitski, J. P. M., Mikkelsen, A. B., Hasholt, B., van den Broeke, M. R., et al. (2017). Substantial export of suspended sediment to the global oceans from glacial erosion in Greenland. *Nature Geoscience*, *10*(11), 859–863. https://doi.org/10.1038/ngeo3046

Painter, S. C., Henson, S. A., Forryan, A., Steigenberger, S., Klar, J., Stinchcombe, M. C., et al. (2014). An assessment of the vertical diffusive flux of iron and other nutrients to the surface waters of the subpolar North Atlantic Ocean. *Biogeosciences*, *11*(8), 2113–2130. https://doi.org/10.5194/bg-11-2113-2014

Pavia, F. J., Anderson, R. F., Pinedo-Gonzalez, P., Fleisher, M. Q., Brzezinski, M. A., & Robinson, R. S. (2020). Isopycnal Transport and Scavenging of 230 Th and 231 Pa in the Pacific Southern Ocean. *Global Biogeochemical Cycles*, *34*(12), e2020GB006760. https://doi.org/10.1029/2020GB006760

Pavia, F. J., Anderson, R. F., Winckler, G., & Fleisher, M. Q. (2020). Atmospheric dust inputs, iron cycling, and biogeochemical connections in the South Pacific Ocean from thorium isotopes. *Global Biogeochemical Cycles*, *34*(9), 1–18. https://doi.org/10.1029/2020GB006562

Pérez-Tribouillier, H., Noble, T. L., Townsend, A. T., Bowie, A. R., & Chase, Z. (2020). Quantifying lithogenic inputs to the Southern Ocean using long-lived thorium isotopes. *Frontiers in Marine Science*, *7*, 207. https://doi.org/10.3389/fmars.2020.00207

Peucker-Ehrenbrink, B. (2018). Land2Sea database (version 2.0) [Dataset]. *PANGAEA*. https://doi.org/10.1594/PANGAEA.892680

Planquette, H., & Sherrell, R. M. (2012). Sampling for particulate trace element determination using water sampling bottles: Methodology and comparison to in situ pumps. *Limnology and Oceanography: Methods*, *10*(5), 367–388. https://doi.org/10.4319/lom.2012.10.367

Poulton, S. W., & Raiswell, R. (2002). The low-temperature geochemical cycle of iron: From continental fluxes to marine sediment deposition. *American Journal of Science*, *302*(9), 774–805. https://doi.org/10.2475/ajs.302.9.774

Rafter, P. (2025). ODV Color Palettes. Retrieved from https://www.prafter.com/color

Robinson, L. F., Belshaw, N. S., & Henderson, G. M. (2004). U and Th concentrations and isotope ratios in modern carbonates and waters from The Bahamas. *Geochimica et Cosmochimica Acta*, *68*(8), 1777–1789. https://doi.org/10.1016/j.gca.2003.10.005

Rowland, G. H. (2025). Thorium concentrations in seawater and sediments at the West Greenland margin, collected during cruise DY081, 2017 [Dataset]. *Zenodo*. https://doi.org/10.5281/zenodo.14807227

Rowland, G. H., Ng, H. C., Robinson, L. F., McManus, J. F., Mohamed, K. J., & McGee, D. (2017). Investigating the use of 232Th/230Th as a dust proxy using co-located seawater and sediment samples from the low-latitude North Atlantic. *Geochimica et Cosmochimica Acta*, *214*, 143–156. https://doi.org/10.1016/j.gca.2017.07.033

Rowland, G. H., Robinson, L. F., Hendry, K. R., Ng, H. C., McGee, D., & McManus, J. F. (2021). The spatial distribution of aeolian dust and terrigenous fluxes in the tropical Atlantic Ocean since the last glacial maximum. *Paleoceanography and Paleoclimatology*, *36*(2), e2020PA004148. https://doi.org/10.1029/2020PA004148

Roy-Barman, M. (2009). Modelling the effect of boundary scavenging on Thorium and Protactinium profiles in the ocean. *Biogeosciences*, *6*(12), 3091–3107. https://doi.org/10.5194/bg-6-3091-2009

Roy-Barman, M., Lemaître, C., Ayrault, S., Jeandel, C., Souhaut, M., & Miquel, J.-C. (2009). The influence of particle composition on Thorium scavenging in the Mediterranean Sea. *Earth and Planetary Science Letters*, *286*(3–4), 526–534. https://doi.org/10.1016/J.EPSL.2009.07.018

Rudnick, R. L., & Gao, S. (2003). Composition of the Continental crust. In *Treatise on Geochemistry* (Vol. 3, pp. 1–64). Elsevier. https://doi.org/10.1016/B0-08-043751-6/03016-4

Rysgaard, S., Boone, W., Carlson, D., Sejr, M. K., Bendtsen, J., Juul-Pedersen, T., et al. (2020). An updated view on water masses on the pan-West Greenland Continental Shelf and their link to proglacial fjords. *Journal of Geophysical Research: Oceans*, *125*(2), e2019JC015564. https://doi.org/10.1029/2019JC015564

Saenko, O. A., Dupont, F., Yang, D., Myers, P. G., Yashayaev, I., & Smith, G. C. (2014). Role of resolved and parameterized eddies in the Labrador Sea balance of heat and buoyancy. *Journal of Physical Oceanography*, *44*(12), 3008–3032. https://doi.org/10.1175/JPO-D-14-0041.1

Santschi, P. H., Adler, D., Amdurer, M., Li, Y.-H., & Bell, J. J. (1980). Thorium isotopes as analogues for "particle-reactive" pollutants in coastal marine environments. *Earth and Planetary Science Letters*, *47*(3), 327–335. https://doi.org/10.1016/0012-821X(80)90019-9

Sarthou, G., Lherminier, P., Achterberg, E. P., Alonso-Pérez, F., Bucciarelli, E., Boutorh, J., et al. (2018). Introduction to the French GEOTRACES North Atlantic Transect (GA01): GEOVIDE cruise. *Biogeosciences*, *15*(23), 7097–7109. https://doi.org/10.5194/bg-15-7097-2018

Schlitzer, R. (2025). Ocean Data View (Version 5.8.2) [Software]. Retrieved from https://odv.awi.de

Schlitzer, R., Anderson, R. F., Dodas, E. M., Lohan, M., Geibert, W., Tagliabue, A., et al. (2018). The GEOTRACES Intermediate Data product 2017. *Chemical Geology*, *493*, 210–223. https://doi.org/10.1016/J.CHEMGEO.2018.05.040

Schroth, A. W., Crusius, J., Sholkovitz, E. R., & Bostick, B. C. (2009). Iron solubility driven by speciation in dust sources to the ocean. *Nature Geoscience*, *2*(5), 337–340. https://doi.org/10.1038/ngeo501

Shen, Z., Zhang, R., Ren, J., Marsay, C., Zhu, Z., Wu, Y., et al. (2024). Distribution of dissolved aluminum and dissolved iron in Kongsfjorden: A glacial fjord in the Arctic. *Marine Chemistry*, *263–264*, 104399. https://doi.org/10.1016/J.MARCHEM.2024.104399

Sherrell, R. M., Annett, A. L., Fitzsimmons, J. N., Roccanova, V. J., & Meredith, M. P. (2018). A "shallow bathtub ring" of local sedimentary iron input maintains the Palmer Deep biological hotspot on the West Antarctic Peninsula shelf. *Philosophical Transactions of the Royal Society A: Mathematical, Physical and Engineering Sciences*, *376*(2122), 20170171. https://doi.org/10.1098/rsta.2017.0171

Shoenfelt, E. M., Winckler, G., Annett, A. L., Hendry, K. R., & Bostick, B. C. (2019). Physical weathering intensity controls bioavailable primary Iron(II) silicate content in major global dust sources. *Geophysical Research Letters*, *46*(19), 10854–10864. https://doi.org/10.1029/2019GL084180

Steenfelt, A. (2012). Rare earth elements in Greenland: Known and new targets identified and characterised by regional stream sediment data. *Geochemistry: Exploration, Environment, Analysis*, *12*(4), 313–326. https://doi.org/10.1144/geochem2011-113

Tagliabue, A., & Arrigo, K. R. (2005). Iron in the Ross Sea: 1. Impact on CO_2 fluxes via variation in phytoplankton functional group and non-Redfield stoichiometry. *Journal of Geophysical Research*, *110*(C3), C03009. https://doi.org/10.1029/2004JC002531

Taylor, S. R., & McLennan, S. M. (1995). The geochemical evolution of the continental crust. *Reviews of Geophysics*, *33*(2), 241–265. https://doi.org/10.1029/95RG00262

Tonnard, M., Planquette, H., Bowie, A. R., Van Der Merwe, P., Gallinari, M., Desprez De Gésincourt, F., et al. (2020). Dissolved iron in the North Atlantic Ocean and Labrador Sea along the GEOVIDE section (GEOTRACES section GA01). *Biogeosciences*, *17*(4), 917–943. https://doi.org/10.5194/bg-17-917-2020

Venchiarutti, C., van der Loeff, M. R., & Stimac, I. (2011). Scavenging of 231Pa and thorium isotopes based on dissolved and size-fractionated particulate distributions at Drake Passage (ANTXXIV-3). *Deep Sea Research Part II: Topical Studies in Oceanography*, *58*(25–26), 2767–2784. https://doi.org/10.1016/J.DSR2.2010.10.040

von Friesen, L. W., & Riemann, L. (2020). Nitrogen fixation in a changing Arctic Ocean: An overlooked source of nitrogen? *Frontiers in Microbiology*, *11*, 3149. https://doi.org/10.3389/FMICB.2020.596426/BIBTEX

Wadham, J. L., Hawkings, J. R., Tarasov, L., Gregoire, L. J., Spencer, R. G. M., Gutjahr, M., et al. (2019). Ice sheets matter for the global carbon cycle. *Nature Communications*, *10*(1), 3567. https://doi.org/10.1038/s41467-019-11394-4

Wilson, J. D., Andrews, O., Katavouta, A., de Melo Viríssimo, F., Death, R. M., Adloff, M., et al. (2022). The biological carbon pump in CMIP6 models: 21st century trends and uncertainties. *Proceedings of the National Academy of Sciences of the United States of America*, *119*(29), e2204369119. https://doi.org/10.1073/pnas.2204369119

Xu, H., & Weber, T. (2025). Quantifying lithogenic inputs to the Ocean from the GEOTRACES thorium transects in a data-assimilation model. *Global Biogeochemical Cycles*, *39*(6), e2024GB008485. https://doi.org/10.1029/2024GB008485

Yu, H., Tan, Q., Chin, M., Remer, L. A., Kahn, R. A., Bian, H., et al. (2019). Estimates of African dust deposition along the trans-atlantic transit using the decadelong record of aerosol measurements from CALIOP, MODIS, MISR, and IASI. *Journal of Geophysical Research: Atmospheres*, *124*(14), 7975–7996. https://doi.org/10.1029/2019JD030574

Zhou, Y., & McManus, J. F. (2024). Heinrich event ice discharge and the fate of the Atlantic Meridional Overturning Circulation. *Science*, *384*(6699), 983–986. https://doi.org/10.1126/science.adh8369

References From the Supporting Information

Abernathey, R. P., & Marshall, J. (2013). Global surface eddy diffusivities derived from satellite altimetry. *Journal of Geophysical Research: Oceans*, *118*(2), 901–916. https://doi.org/10.1002/jgrc.20066

Andrews, J. T., & Syvitski, J. P. M. (1994). Sediment fluxes along high-latitude glaciated Continental margins Northeast Canada and Eastern Greenland. In *Material fluxes on the surface of the earth* (pp. 99–115). National Academy Press.

Bourne, M. D., Thomas, A. L., Mac Niocaill, C., & Henderson, G. M. (2012). Improved determination of marine sedimentation rates using 230 Th xs. *Geochemistry, Geophysics, Geosystems*, *13*(9), Q09017. https://doi.org/10.1029/2012GC004295

Causse, C., & Hillaire-Marcel, C. (1989). Thorium and Uranium Isotopes in Upper Pleistocene Sediments of ODP Sites 645 (Baffin Bay), 646, and 647 (Labrador Sea). *Proceedings of the Ocean Drilling Program, Scientific Results*, *105*(29), 551–560. https://doi.org/10.2973/odp.proc.sr.105.155.1989

DePaolo, D. J., Maher, K., Christensen, J. N., & McManus, J. (2006). Sediment transport time measured with U-series isotopes: Results from ODP North Atlantic drift site 984. *Earth and Planetary Science Letters*, *248*(1–2), 394–410. https://doi.org/10.1016/J.EPSL.2006.06.004

European Union. (2025). GLORYS12V1 [Dataset]. *Copernicus Marine service information (CMEMS) Marine Data Store (MDS)*. https://doi.org/10.48670/moi-00021

Gariepy, C., Ghaleb, B., Hillaire-Marcel, C., Mucci, A., & Vallieres, S. (1994). Early diagenetic processes in Labrador Sea sediments: Uranium-isotope geochemistry. *Canadian Journal of Earth Sciences*, *31*(1), 28–37. https://doi.org/10.1139/e94-004

Henderson, G. M., Heinze, C., Anderson, R. F., & Winguth, A. M. E. E. (1999). Global distribution of the 230Th flux to ocean sediments constrained by GCM modelling. *Deep-Sea Research Part I Oceanographic Research Papers*, *46*(11), 1861–1893. https://doi.org/10.1016/S0967-0637(99)00030-8

Hillaire-Marcel, C., Aksu, A., Causse, C., de Vernal, A., & Ghaleb, B. (1990). Response of Th/U in deep Labrador Sea sediments (ODP Site 646 to changes in sedimentation rates and paleoproductivities. *Geology*, *18*(2), 162–165. https://doi.org/10.1130/0091-7613(1990)018<0162:ROTUID>2.3.CO;2

Hvid Ribergaard, M., Anker Pedersen, S., Ådlandsvik, B., & Kliem, N. (2004). Modelling the ocean circulation on the West Greenland shelf with special emphasis on northern shrimp recruitment. *Continental Shelf Research*, *24*(13–14), 1505–1519. https://doi.org/10.1016/J.CSR.2004.05.011

Lilly, J. M., Rhines, P. B., Schott, F., Lavender, K., Lazier, J., Send, U., & D'Asaro, E. (2003). Observations of the Labrador Sea eddy field. *Progress in Oceanography*, *59*(1), 75–176. https://doi.org/10.1016/J.POCEAN.2003.08.013

Lindborg, T., Rydberg, J., Tröjbom, M., Berglund, S., Johansson, E., Löfgren, A., et al. (2016). Biogeochemical data from terrestrial and aquatic ecosystems in a periglacial catchment, West Greenland. *Earth System Science Data*, *8*(2), 439–459. https://doi.org/10.5194/essd-8-439-2016

Ohnemus, D. C., & Lam, P. J. (2015). Cycling of lithogenic marine particles in the US GEOTRACES North Atlantic transect. *Deep Sea Research Part II: Topical Studies in Oceanography*, *116*, 283–302. https://doi.org/10.1016/J.DSR2.2014.11.019

Prater, M. D. (2002). Eddies in the Labrador Sea as observed by profiling RAFOS floats and remote sensing. *Journal of Physical Oceanography*, *32*(2), 411–427. https://doi.org/10.1175/1520-0485(2002)032<0411:EITLSA>2.0.CO;2

Tepe, N., & Bau, M. (2015). Distribution of rare earth elements and other high field strength elements in glacial meltwaters and sediments from the western Greenland Ice Sheet: Evidence for different sources of particles and nanoparticles. *Chemical Geology*, *412*, 59–68. https://doi.org/10.1016/J.CHEMGEO.2015.07.026

Zhou, Y., McManus, J., Jacobel, A., Costa, K., Wang, S., & Caraveo, B. (2020). Enhanced iceberg discharge in the western North Atlantic during all Heinrich events of the last glaciation. https://doi.org/10.31223/OSF.IO/YN57Z